Study of wine samples by laser-induced breakdown spectroscopy

Jana Bocková[1,2*]

Supervisor: Pavel Veis[1†]

[1] Department of Experimental Physics, Mlynská Dolina, 842 48 Bratislava, Slovakia
[2] Institut Lumière Matière, UMR5306 – Université Lyon 1-CNRS, 69622 Villeurbanne CEDEX, France

Abstract: This work introduces novel approach to the analysis of liquid samples with organic background, such as wine, by laser-induced breakdown spectroscopy (LIBS). The work is aimed at the development of sample preparation procedure suitable for the analysis of such liquids by LIBS as the initiation of laser-induced plasma in bulk liquids is a complex issue due to the complications accompanying such analysis, e.g. bubble and shock wave formation, plasma quenching, etc. Sample preparation procedure has been developed in cooperation with prof. Jin Yu at Institut Lumière Matière (ILM), Lyon, France. Its analytical performance and the application to the analysis of elemental composition of wines of different origin has been tested at ILM, Lyon, France and at Faculty of Mathematics, Physics and Informatics of Comenius University in Bratislava (FMFI UK), Slovakia as well. Here, we present the results of the work that has been performed at FMFI UK, Bratislava, Slovakia, which actually follows the work already done at ILM, Lyon, France, results of which have been already submitted for publication titled "Determination of metal elements in wines using surface-assisted laser-induced breakdown spectroscopy" (Bocková et al., 2016).

Keywords: LIBS, wine, elemental composition

Introduction

Elemental analysis of liquids finds its application in numerous areas, such as food industry, drinking water quality control, cosmetics, pharmacy, medicine, etc. There are several spectrochemical techniques, such as atomic absorption spectroscopy (AAS), inductively coupled plasma optical emission spectroscopy (ICP-OES), inductively coupled plasma mass spectrometry (ICP-MS), etc., that have been successfully applied to such analysis reaching limits of detection (*LOD*s) of up to $10^{-3}\,\mu g/l$. However, the main drawback of these methods lies in complex sample pretreatment procedures often lasting for long-hours and requiring the use of one or more of the following chemicals, such as HNO_3, HCl, H_2O_2, etc., in order to reduce possible matrix interferences. Thus, there is a tendency to establish a method for simple and fast elemental analysis of liquids with minimal sample preparation without the use of any chemical reagents that would be possible to apply on-site. We introduce one that meets all of the above-mentioned requirements, i.e. laser-induced breakdown spectroscopy (LIBS). Despite its growing popularity since its invention in 1963, this technique has been applied mainly to solid and gaseous sample analysis and relatively smaller number of researchers devoted their studies to liquid samples. This lack of studies is mainly due to the experimental difficulties related to the analysis of liquids. Laser-induced breakdown inside or on the surface of liquids is a process with low efficiency as a large portion of laser energy is being used for evaporation subsequently leading to cavitation. Moreover, expanding plasma compresses surrounding liquids, and thus induces the formation of shock waves. Focusing the laser pulse on the surface of liquids causes splashes degrading the focusing optics. These phenomena, therefore, decrease the analytical performance of the method for liquid analysis. In order to overcome the above-mentioned difficulties related to laser-induced plasma in bulk liquids, several alternative configurations have been proposed. We describe them briefly below. Subsequently, we give the overview of the methods already applied to LIBS analysis of wines. Finally, we describe our method for wine analysis and demonstrate the preliminary results.

1 General principle of LIBS

Laser-induced breakdown spectroscopy (LIBS) represents an analytical technique using dielectric

*bockova10@uniba.sk
†pavel.veis@fmph.uniba.sk

breakdown induced by optical radiation for the determination of elemental composition of a sample.

The ability to produce electric breakdown in low-pressure gas tubes with or without electrodes at frequencies from around hundreds of kilohertz to tens of megahertz had been known for at least 100 years prior to the development of lasers in 1960. Later on, microwave-range electromagnetic fields with frequencies on the order of gigahertz were used to produce breakdown of gases at reduced pressures. Experiments were performed at reduced pressures, because breakdown threshold exhibits its minimum in rarefied gases. In the case of static or microwave fields at atmospheric pressure, the electric field of tens of kilovolts per centimetre is required, while at optical frequencies even much stronger fields of around tens of megavolts per centimetre are required. As common optical sources do not provide us such strong electric fields, a crucial point was the invention of a Q-switched laser in 1963 capable of producing a pulsed output beam with short-duration laser pulses (femtoseconds to nanoseconds) of high peak power (gigawatts). This became a foundation stone of LIBS technique (Miziolek, 2006).

In the past decades, many other analytical techniques, such as atomic absorption spectroscopy (AAS), atomic emission spectroscopy (AES), inductively coupled plasma mass spectrometry (ICP-MS), etc., achieved popularity thanks to their low detection limits (up to sub-ppb levels). Although sensitivity of LIBS (sub-ppm levels) is lower compared to the above-mentioned techniques, it still holds an important position due to its inherent advantages:

- possible to analyse solid, liquid or gaseous samples, and aerosols,
- capability to provide measurements in gaseous and liquid environment of any type and pressure,
- minimal sample preparation,
- in-situ measurements in real-time,
- flexibility of experimental setup configurations,
- remote analysis (for distances of up to about $100\,m$),
- relatively low cost compared to other analytical techniques.

Let us briefly describe basic principle of LIBS. LIBS is initiated by focusing a high-energy laser pulse on the surface or inside a sample. The leading edge of the laser pulse immediately interacts with the target material, evaporating and ionising a small quantity of the sample. Optical power converted to the kinetic energy of emerged electrons leads to fast growth of free electron density at the focal point and further absorption of the trailing edge of the laser pulse. As a result of it, the existing vapour heats up and expands, ablating more sample material. After the laser pulse termination, ions and electrons recombine, and characteristic spectra of the sample material are observed due to radiative relaxation and the originated plasma cools down (Järvinen, 2013). Example scheme of LIBS experimental setup is in Fig. 5.

In general, LIBS experiments are comprised of three fundamental steps, i.e. plasma formation, signal collection and data evaluation. All of these steps stand for complex issues that affect analytical performance of the method. Plasma formation induced by laser pulse is a phenomenon depending on laser pulse characteristics on the one hand, and on the state of aggregation of the irradiated sample, its physical and chemical properties on the other hand. Laser-induced breakdown has, therefore, distinct progress in solids, liquids, gasses and aerosols. We deal with laser-induced plasma of liquids in section 2.1 Laser-induced breakdown in liquids, in more detail (De Giacomo, 2012).

Signal collection is ensured by spectrometers equipped with detectors. Demands for spectrometers used in LIBS setups include possibility of fast synchronization, reasonable spectral coverage in ultraviolet and visible range as well as resolution suitable for atomic spectroscopy ($< 0.1\,nm$). The detectors should have quite sensitive array, so that gate delays (GD) of several μs provide good signal-to-noise ratio (SNR) spectra enabling the analysis with low (sub-ppm) limits of detection, LODs, (Galbács, 2015).

LIBS as a spectrochemical method may be used for qualitative as well as quantitative analysis. Qualitative analysis is often performed with the help of spectral line databases, such as NIST (National Institute of Standards and Technology) atomic spectra database or Atomic spectral line database from CD-ROM 23 of R. L. Kurucz. Quantitative analysis aimed at concentration determination may be performed either by using internal standards, calibration curves or calibration free LIBS (Lazic, 2014).

2 Liquid analysis by LIBS

First investigations of laser-induced plasma in liquids were performed in 1963, i.e. in the same year as LIBS technique was developed. Buzukov et al. (1969) were first to consider generating plasma in bulk water. As laser-induced breakdown in bulk liquids exhibits specific features (described below), further studies were focused on shock wave formation and cavity vaporisation in bulk liquids as well as alternative configurations of liquid analysis by LIBS (Cremers, 2006).

2.1 Laser-induced breakdown in liquids

The interaction of laser light with irradiance below the breakdown-threshold with liquids is accompanied by phenomena, such as coherent scattering (stimulated Raman and/or Brillouin scattering), self-focusing, medium heating and production of "quasi-free" electrons by photolysis. On the other hand, the interaction of high-irradiance laser ($\approx 10^{12} Wcm^{-2}$) with liquids is accompanied by phenomena, such as non-linear effects, molecule orientation, liquid contraction, electron hydration, laser filamentation and white light generation.

Laser-induced breakdown in bulk liquids is initiated by cascade ionisation and multiphoton ionisation induced by high-energy laser pulses. Cascade ionisation is the process activated by seed free electrons already present in the focal volume. The electromagnetic field generated by laser light causes oscillations of these free electrons. This results in their collisions with nearby heavy particles (such as atoms or molecules). During these collisions, free electrons may absorb laser light energy, which leads to the process named inverse Bremsstrahlung absorption. The role of the heavy particles in the process of Bremsstrahlung absorption is to preserve momentum and energy. When a free electron gains energy high enough to ionise a bound electron, their collision results in the production of two free electrons of lower energies. Repetition of this process leads to electron cascade (breakdown). The mechanism of the two-body collision by which the population of free-electrons is multiplied is known as impact ionisation, and may happen only when the energy losses caused by inelastic collisions, electron-ion recombinations and diffusion of electrons out of the focal volume are smaller than the energy absorption in the same place.

Multiphoton ionisation is a non-linear process and requires higher energy densities rather than cascade ionisation. Due to this fact, for *ns* laser pulses, cascade ionisation is a dominant breakdown mechanism, except for pure liquids not containing seed free electrons. In the process of multiphoton ionisation, several photons of energies lower than ionisation potential are combined to ionise an atom, thus there is no need of the presence of seed free electrons (i.e. impurities inside liquids). Electron formation induced by multi-photon ionisation may cause rearrangement of water molecules (consisting in charged particles, hydrated electrons and counterions). The hydration process decreases the kinetic energy that a free electron gains through the absorption of laser light, and thus increases the breakdown threshold.

The threshold irradiance for laser-induced breakdown in liquids is, therefore, determined by the properties of a medium, such as ionisation energy, type and concentration of impurities, and within a given medium it depends on laser beam characteristics, such as wavelength, pulse width, focusing angle and beam diameter. In general, the breakdown threshold in liquids is substantially higher with respect to air and solids as a large portion of laser pulse energy is spent in mechanical effects described below (De Giacomo, 2007; Lazic, 2014).

2.2 Laser-induced cavitation, shock wave formation and plasma stability in bulk liquids

Once the plasma is formed, it starts to expand at supersonic velocity (of the order of $10^5 cms^{-1}$), compresses the surrounding liquid creating a shock wave (with pressure in excess of $100 MPa$) and rapidly extinguishes. Compared to air, liquids are less compressible, which causes the confinement of plasma and considerably higher local temperatures and pressures. A significant amount of the high-temperature plasma energy is transferred to the surrounding liquid (plasma extinguishes fast) resulting in its evaporation. Subsequently, the local liquid evaporation continues and causes almost adiabatic expansion of the vapour resulting in the bubble formation. Bubbles expand until their pressure becomes lower than the pressure of the surrounding liquid medium. The kinetic energy of the liquid at the time of bubble expansion has been transformed into its potential en-

ergy

$$E_b = \frac{4\pi}{3}(p_0 - p_v) R_{\max}^3 \quad (1)$$

where p_0 is the hydrostatic pressure, p_v is the vapour pressure inside the bubble and $R_{\max}$ is the maximum radius of a fully expanded bubble.

Another consequence of the confinement is the increase in the rate of recombination phenomenon. Plasma persists for a shorter time (few hundreds of *ns*) and the emission spectra show broad continuum as a result of fast recombination and partially of the Bremsstrahlung emission.

Such a strong interaction between the plasma and the surrounding medium reduces quantitative capabilities of LIBS technique. Practically, the only detectable signal is broad continuum that exhibits blackbody spectrum and can be described by the following equation

$$I(\lambda,\, T) = I_0 C \lambda^{-5} (e^{\frac{hc}{\lambda kT}} - 1)^{-1} \quad (2)$$

where T is the temperature of plasma, h is the Planck constant, c and λ is the speed and wavelength of light, k is the Boltzmann constant and C is a constant. Although it carries information about electron temperature, it almost lacks spectroscopic information (De Giacomo, 2007). For low-energy transitions, it is possible to detect spectroscopic signals, however, they often suffer from significant self-absorption, short lifetimes and are extremely broadened due to the quenching and confinement of the surrounding liquid.

Furthermore, LIBS measurements of bulk liquids deal with extremely unstable signals because of the probabilistic character of breakdown, of which threshold significantly depends on the impurities present. Dissolved gases also contribute to the instabilities as they may lead to beam scattering and may be preferable loci for the breakdown formation (De Giacomo, 2012; Lazic, 2014).

De Giacomo et al. (2004) generated laser-induced plasma in the bulk of four different water solutions ($AlCl_3$, $NaCl$, $CaCO_3$ and LiF) in order to study their emission signals. Fig. 1 shows temporal evolution of $Al\,I$ lines at $394.40\,nm$ and $396.15\,nm$. We can observe strong continuum after $100\,ns$ from the laser pulse due to fast recombination and Bremsstrahlung emission. $50\,ns$ later, strong continuum declines and $Al\,I$ emission lines appear. The evidence that plasma persists for a short time is that $200\,ns$ after the ignition of the laser spark, the emission signal virtually disappears. De Giacomo et al. did not observe any spectral lines in the range of $250 - 700\,nm$ corresponding to transitions between higher energy levels as a result of fast plasma cooling, neither ionic lines due to fast electron-ion recombination that came before the decay of the continuum signal. They concluded that bulk liquid analysis by LIBS technique is not appropriate for quantitative analysis as it requires many accumulations of laser pulses and can not detect all of the elements present in a liquid sample.

2.3 Alternative ways of liquid analysis by LIBS

Despite the above-mentioned difficulties related to the LIBS analysis of bulk liquids, intensive research has been done in this area as the analysis of liquids is required in multiple fields, such as medicine, pharmacy, cosmetics, food industry, drinking water quality control, environmental pollution monitoring, nuclear industry, etc. In order to avoid these obstacles, innovative approaches in liquid analysis by LIBS technique have been applied. The first approach is to apply a more appropriate experimental configuration, while the second one is the transformation of a liquid sample to a solid or a "quasi-solid" sample providing the measurements with unmodified experimental LIBS apparatus (Jantzi, 2016).

2.3.1 Modified experimental LIBS configurations

However, it is possible to analyse liquids in their original liquid state, in order to obtain results that are possible to interpret, there is a need to reorganize LIBS experimental apparatus into one of the following configurations: double pulse LIBS, surface analysis of static bulk liquids, liquid jets, isolated micro-droplets formation, nebulization into aerosols, etc. The advantage of the last three mentioned techniques over the other two techniques is that plasma expands in a gaseous environment instead of in the liquid one, and thus the rapid plasma confinement phenomenon is avoided (Janzen, 2005).

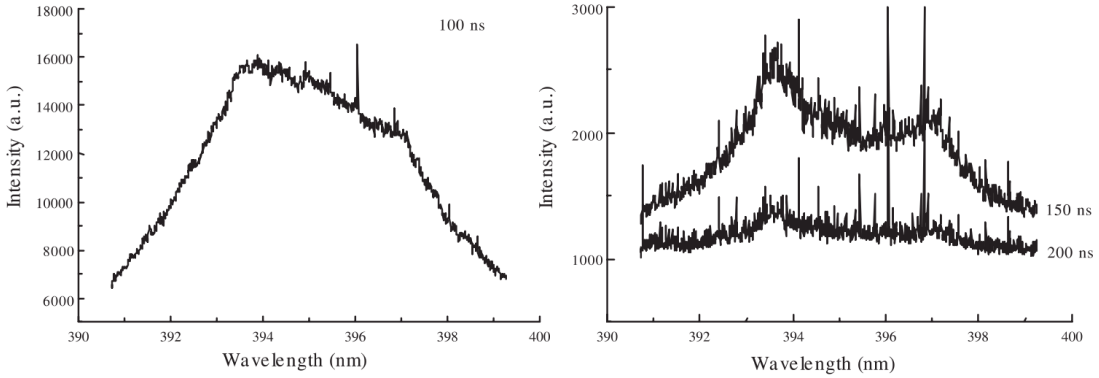

Fig. 1: Temporal evolution of Al I (394.40 nm and 396.15 nm) lines in $AlCl_3$ water solution at 100 ns, 150 ns and 200 ns gate delay (GD) times; laser energy 400 mJ, gate width (GW) 100 ns, three accumulations, 100 laser pulses (De Giacomo, 2004).

Double pulse LIBS of bulk liquids

Double pulse LIBS (DP-LIBS), firstly introduced in 1984, is mostly suitable for the analysis of liquids with a relatively low-boiling point (e.g. water). The main advantage of this technique is higher sensitivity and higher stability of emission signal that can be up to two orders of magnitude higher compared to single pulse LIBS (SP-LIBS).

We assume that there are two main effects contributing to the advancement of the emission signal:

- A greater amount of ablated matter as a consequence of the fact that the first laser pulse increases the temperature of the target surface, leading to the decrease of its reflectivity and increase of the penetration depth, subsequently resulting in a more efficient ablation by the second laser pulse.

- Higher average temperature and more stable signal as a result of the longer decay time due to the slower energy transfer from plasma to the surrounding medium as the second pulse expands in a rarefied environment of very high temperature, i.e. thousands Kelvin (De Giacomo, 2007).

In bulk liquids, the enhancement of the emission signal when using DP-LIBS is either due to the excitation (by the second laser pulse) of a weak plasma generated in a vapour bubble by the first laser pulse, or due to the generation of a plasma in a vapour bubble instead of in a liquid medium (Galbács, 2015).

De Giacomo et al. (2005) studied tap water with Na and Mg dissolved cations by DP-LIBS in collinear configuration. In Fig. 2 we can compare the spectrum obtained after the first laser pulse representing a strong continuum (continuous line) with the spectrum obtained after the second laser pulse (dotted line). The second laser pulse initiated plasma in the water bubble created by the first laser pulse, thus we can observe rich line emissions from Na atoms at wavelengths 588.99 nm and 589.59 nm. The limits of detection (LODs) of Mg and Na were determined to be 1.4 mg/l and 0.4 mg/l, respectively. As the intensity threshold in water is closely related to the solute amount (see section 2.1 Laser-induced breakdown in liquids), different concentrations of solute can cause differences in plasma parameters (such as electron number density, ionisation degree and excitation temperature), which may limit the range, in which the intensity of a spectral line and concentration follow linear trend (Radziemski, 1989).

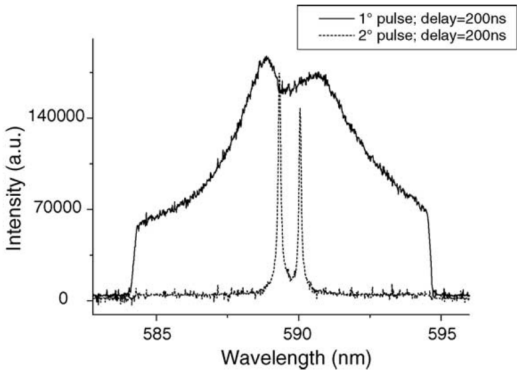

Fig. 2: Comparison of the first (continuous line) and second laser pulse spectra (dotted line) of NaI lines; laser energy 100 mJ, GD 200 ns, GW 500 ns, number of accumulations 100 (De Giacomo, 2005).

Surface analysis of static bulk liquids

In a classical LIBS configuration used for solid sample analysis, laser beam is directed perpendicularly to the sample surface, which in the case of liquids results in splashing of the liquid, and thus polluting the focusing optics. The explanation is that at atmospheric pressure, plasma expands perpendicularly to the sample surface. This phenomenon can be, however, reduced by using a tilted configuration for the surface analysis of static bulk liquids (Fichet, 2001).

Fichet et al. (2001) performed quantitative elemental analysis of water and oil samples by using the LIBS configuration, in which the laser beam was focused at an angle of 15° to the surface of a static liquid sample in the ablation cell in order to avoid the pollution of focusing optics by splashing. Lowering of laser pulse frequencies to $1\,Hz$ minimized the perturbations following the laser pulses, and thus increased the reproducibility of measurements. Standard aqueous and oil solutions containing 12 elements, i.e. *Pb*, *Si*, *Ca*, *Na*, *Zn*, *Sn*, *Al*, *Cu*, *Ni*, *Fe*, *Mg* and *Cr*, were diluted with distilled water and pure oil to obtain samples in the concentration range of $50-2000\,\mu g/ml$ and $50-900\,\mu g/ml$, respectively. Emission lines were detected by using THR 1000, Jobin-Yvon spectrometer. Calibration curves were plotted to determine *LOD*s that were in the range from $0.3\,\mu g/ml$ (for *Ca*) to $120\,\mu g/ml$ (for *Zn*) in water samples and from $0.3\,\mu g/ml$ (for *Ca*) to $130\,\mu g/ml$ (for *Zn*) in oil samples. Subsequently, an echelle spectrometer was used to study *LOD*s of *Al* in water, which was determined to be $30\,\mu g/ml$. The analytical reproducibility obtained by using THR spectrometer for water and oil samples was found to be around 3% and for water samples by using the echelle spectrometer was found to be around 10%.

Liquid jets

Liquid jets represent an alternative way of liquid analysis by LIBS, where the problem of splashing is avoided by focusing the laser beam onto the surface of a flowing liquid. Compared to surface analysis of static liquids, liquid jets enable to increase the rate of elemental analysis as well as to increase the reproducibility of measurements due to the possibility to present fresh sample to successive laser pulses (Yaroshchyk, 2005).

Yaroshchyk et al. (2005) compared the sensitivity of LIBS in the laminar liquid jet configuration with the one of the surface analysis of static liquids. The *LOD*s of *Na*, *Mg*, *Al*, *Ca*, *Ti*, *V*, *Cr*, *Mn*, *Ni*, *Fe*, *Cu*, *Zn*, *Mo*, *Ag*, *Cd* and *Ba* were determined to be on average 4-times lower (in the range of $10^{-1}-10^{1}\,ppm$) in the case of using liquid jet configuration compared to the surface analysis of static liquids. Lower sensitivity of surface analysis of static liquids was explained by micro-splashes degrading focusing optics as well as by thermal effects caused by the continuous ablation of the same spot. Finally, analytical performance of the liquid jet configuration was compared with the one of ICP-OES in the study of lubricating oil samples. For the liquid jet experiment, there was a need to dilute two samples with a blank oil in order to ensure free current through a nozzle. On the other hand, acidification and microwave digestion of the samples was necessary prior to the analysis by ICP-OES. The results obtained by the above-mentioned methods were comparable, except for one sample, for which concentrations of *Cu*, *Mg*, *Mn* and *Na* were close to theoretically estimated *LOD*s of the LIBS experimental setup used for measurements.

Analysis of aerosols and isolated micro-droplets

Another approach to prepare liquid samples for LIBS analysis is the formation of small droplets or aerosols by nebulization techniques (e.g. pneumatic, ultrasonic and electrospray nebulization). LIBS is considered to be well suited for the analysis of aerosols and small droplets due to discrete nature of LIBS plasma volume on the one hand and discrete nature of aerosol particles on the other hand (Musazzi, 2014).

Aras et al. (2012) used ultrasonic nebulization sample-introduction system that uses a piezoelectric crystal vibrating at frequencies of $2.4\,MHz$ for conversion of a liquid sample into aerosol droplets of about $1-20\,\mu m$ in diameter. Subsequently, a tandem heater-condenser membrane dryer unit was used for desolvation and drying of aerosols prior to laser ablation. Laser energy, sample and drying gas flow rate, and detector timing parameters were studied in order to optimize conditions for LIBS measurements. In Fig. 3 we can observe the enhancement of the emission signal of *PbI* lines (approximately by the factor of 3) caused by the application of a naphion membrane dryer, selective to moisture content of the sample that passes through the dryer. The evidence of water content reduction is supported by the de-

crease in the emission signal of HI in the presence of the membrane dryer. A set of calibration standards was prepared by solution of chloride or nitrate salts of Na, K, Mg, Ca, Cu, Al, Cr, Cd, Pb and Zn in ultrapure water. *LOD*s were determined to be in the range from $1.0\,mg/l$ (for Mg) to $82.3\,mg/l$ (for Cd) without using membrane dryer and from $0.45\,mg/l$ (for Na) to $43.99\,mg/l$ (for Cd) in the presence of membrane dryer. Finally, the applicability of the system was tested on real water samples with mean recoveries in the range of around $79.7 \pm 24.4 - 118.8 \pm 40.9\,mg/l$.

2.4 Transformation of a liquid sample to a solid or a "quasi-solid" sample

In order to overcome the drawbacks of bulk liquid analysis by LIBS technique (see section 2.2 Laser-induced cavitation, shock wave formation and plasma stability in bulk liquids) and accomplish the advantages of solid target analysis, transformations of liquids to a solid or "quasi-solid" state have arisen. In fact, there are several ways of possible transformations, i.e. substrate absorption, liquid-to-solid matrix conversion, liquid layer on solid matrix and freezing.

Substrate absorption

Substrate absorption is a method of liquid analysis in a solid matrix configuration based on depositing a small volume of a liquid sample onto a porous solid substrate and spontaneous drying under ambient conditions. The remains of liquid samples are then ablated by laser pulse together with the solid substrate, therefore it is necessary to choose the substrate that would not cause any contamination or spectral interferences. Sample preparation is a relatively fast procedure requiring only few minutes, thus it can be applied on-site. Compared to bulk liquid analysis, substrate absorption method significantly improves analytical performance due to better laser-to-solid interaction. Furthermore, it exhibits only a little or almost no matrix effects and offers the possibility to use internal standard normalization (Jantzi, 2016).

Yaroshchyk et al. (2005) investigated the possibility of using paper substrates for SP- and orthogonal pre-ablation DP-LIBS analysis of engine oils. They studied *LOD*s of the following metallic elements: Fe, Ag, Al, Cr, Cu, Ni, Ti, Mo, Zn, Pb, Si, V and Cd. *LOD*s for all of the studied elements were in low-ppm range ($10^0 - 10^1\,ppm$). Relatively low benefit of using DP-LIBS (approximately 2-times) over SP-LIBS was evaluated to be not substantially significant to decide for DP-LIBS when taking into consideration also the complexity and cost of DP-LIBS system compared to SP-LIBS system.

Liquid-to-solid matrix conversion

Up till now many different approaches have been used to convert liquid solutions into solid-matrix samples. Such pre-concentration processes enable us to reach sub-ppm level *LOD*s for studied elements. We introduce them in more detail further.

Bae et al. (2015) focused on studying of a small amount of liquid samples such as single droplet ($15\,\mu l$ volume) by SENLIBS method. They described the problem of inhomogeneous distribution of dried residues in a very small area (of the order of $10^1\,\mu m$ in diameter) that requires proper control of laser ablation location. In order to avoid these difficulties, this research group devised a new solid substrate for liquid analysis of a small amount of a liquid sample by patterning a silicon wafer with a laser. It resulted in 40×40 crossed trenches ($1\,cm$ long, $\sim 19\,\mu m$ wide and $\sim 10\,\mu m$ deep) on the surface of a laser-patterned silicon wafer (LPSW) effectively trapping the liquid samples to be analysed and providing more homogeneous distribution of studied elements. They studied liquid samples with different concentrations of K (in the range of $2 - 25\,ppm$) and constant concentration of Rb ($5\,ppm$) on the LPSW as well as on a bare silicon wafer (SW). In general, the relative standard deviation (*RSD*) of the intensity of an analyte emission signal decreases with increasing concentration of the analyte as there is a strong positive correlation between the analyte emission signal intensity and its concentration, while in contrast, fluctuations have only a negligible correlation with the concentration. However, Bae et al. observed that *RSD* of the intensity ratio of KI ($766.490\,nm$) and RbI ($780.027\,nm$) had tendency to increase for K concentrations higher than $10\,ppm$ (see Fig. 4). They explain this phenomenon by heterogeneous spectral intensity saturation effect due to the heterogeneous distribution of analytes on the surface of a solid substrate (more intense for SW than for LPSW) and propose a potential solution to this problem by spreading a liquid sample over a larger area. The obtained *LOD*s of K were $0.75\,ppm$ and $0.60\,ppm$ for SW and LPSW, respectively. In comparison with SW, using LPSW as a solid substrate seems to bring about the increase in sampling efficiency for LIBS analysis and

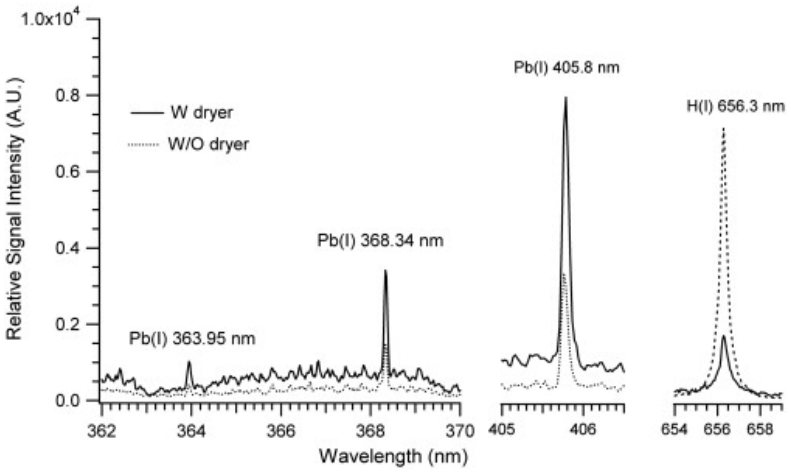

Fig. 3: Comparison of emission lines of PbI (363.95 nm; 368.34 nm and 405.8 nm) and HI (656.3 nm) with (continuous line) and without (dotted line) using a membrane dryer; laser energy, GD, GW and number of accumulations are not explicitly specified (Aras, 2012).

the improvement of linear dynamic range of calibration curves as well as precision of the analysis.

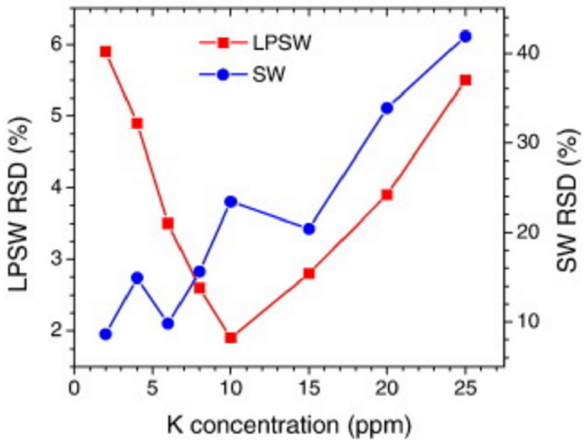

Fig. 4: Comparison of the RSD values of the intensity ratio of KI (766.490 nm) and RbI (780.027 nm) lines as a function of K concentration for SW (blue line) and LPSW (red line) substrates; laser energy 40 mJ, GD 500 ns, GW 1.05 ms, number of accumulations not explicitly specified (Bae, 2015).

Liquid layer on solid matrix

This technique represents an alternative sample preparation method for indirect analysis of viscous liquids by LIBS. It is based on the deposition of gel-like viscous liquid onto the surface of a metallic target resulting in a homogeneous few μm thick layer. In the process of laser ablation, the laser pulse is focused slightly under the surface of a metallic target (approximately 1.5 mm), transmits through a transparent liquid layer and generates a dense hot metallic plasma. Metallic plasma interacts with a liquid layer leading to its vaporization and ionisation. Finally, plasma has properties similar to metallic plasma (approximately 15000 K) and contains species embodied in the metallic target, liquid film as well as in the ambient gas (Xiu, 2013; Xiu, 2014).

Xiu et al. (2013) applied the above-mentioned technique to the analysis of cooking oils using an aluminium target. The emission spectrum contained elements evaporated from the target (Al, Si and Fe), elements coming specifically from the viscous oil layer (Na, Ca, C, H and Cl) and an element of the ambient gas (Ar). At 0.5 μs after the initiation of laser pulse, the electron density and plasma temperature were of the order of 1.4×10^{18} cm^{-3} and 1.6×10^4 K, which was marked to be comparable or even higher than the temperature of plasma induced on a pure aluminium target. The high temperature (even at 2 μs remained higher than 1.6×10^4 K) allowed to observe the emission of Cl, which is difficult to be detected by LIBS due to its high excitation energy.

Freezing

To sum up, there are several advantages of the ablation on solids over liquids, such as a reduced threshold laser energy, higher sampling acquisition

rate, higher sensitivity, easier handling, no special changes in the arrangement of experimental apparatus required, etc. Compared to the above-mentioned techniques of substrate absorption, liquid-to-solid matrix conversion and liquid layer on solid matrix, turning a liquid sample into a solid one by freezing brings additional advantages, such as no necessity of the pre-enrichment of sample solutions as well as the risk of plasma pollution by odd elements present in substrate matrix is reduced. The latter is of high importance mainly in the case of multi-elemental analysis of trace metals (Sobral, 2012; Jantzi, 2016).

Cáceres et al. (2001) reported on LIBS analysis of liquids by using a quick-freeze method to convert liquid samples to ice prior to laser ablation. The quick-freeze procedure was based on pouring of $25\,ml$ of water samples doped with known concentrations of Na and Al into a pre-cooled container by liquid nitrogen for $20\,s$ and subsequently continue freezing the sample for another $1\,min$. They managed to optimize experimental conditions for the analysis of frozen samples and reached LODs of the order of $10^0\,ppm$.

3 Elemental analysis of wine

Wine is an alcoholic beverage, which is a product of yeast fermentation of sugars present in grapes or other fruits. From the chemical point of view, it is a complex mater comprising diverse organic as well as anorganic chemical constituents (Jackson, 2008). Tab. 1 summarizes chemical composition of wine.

3.1 Metals in wine, their role and origin

Metals are present in wine in various concentrations. In general, we can sort them according to their concentrations, in which they are present in wine as follows:

1. Major metals ($10^1 - 10^3\,mg/l$) – K, Ca, Mg and Na. In general, K has the highest concentration among the elements present in wine, Ca and Mg have comparable concentrations that are approximately an order of magnitude lower than that of K. Concentration of Na is also comparable or lower than that of Ca and Mg.

2. Minor metals ($10^{-1} - 10^1\,mg/l$) – Al, Cu, Fe, Mn, Rb, Sr and Zn.

3. Trace metals ($10^{-1} - 10^2\,\mu g/l$) – Ba, Cd, Co, Cr, Li, Ni and Pb. The largest dispersions are present in concentration of trace metals, especially in the concentrations of Ni and Pb.

Metals in wine not only influence its organoleptic characteristics, such as flavour, aroma, colour and freshness, but they play important roles in individual stages of wine-making process as well (Pohl, 2007). Roles of particular metals are listed in Tab. 2.

There are several sources of metals present in wines, but in general, the origin of metals is two-fold:

1. Primary (natural) origin – metals coming from soil and reaching wine through grapes. They represent the largest source of metal content in wine, which is also related to the maturity and variety of grapes, the climatic conditions during their growth as well as to the type of soil on which vine is grown. For example, the wines that are grown in coastal regions usually have higher content of Na due to wind bringing marine spray.

2. Artificial origin – associated with external impurities as a result of anthropogenic activities affecting wine not only during growth of grapes, but also during different stages of wine-making (harvesting, bottling, cellaring). This source may be further divided into three subgroups:

   - Application of substances employed in cultivation to protection and growth support – fertilizers cause differences in K and Ca content, and together with pesticides and fungicides increase the content of Cd, Cu, Mn, Pb and Zn. Pesticides may also lead to higher content of As.
   - Pollution of the environment – vineyards located close to road traffic or industrial parks may suffer from higher content of Cd and Pb due to vehicle-exhaust fumes as well as industrial waste and emissions causing air, water and soil pollution.
   - Enological source – contamination in different stages of wine production, e.g. long contact with wine-making machinery, pipes, casks and barrels usually leads to higher amounts of Al, Cd, Cr, Cu, Fe and Zn. Fining and clarifying substances,

Tab. 1: Chemical composition of wine (Jackson, 2008).

Chemical constituent	The most abundant species
water	
alcohols	lower alcohols – ethanol, methanol; higher (fusel) alcohols - hexanol, benzyl alcohol; diols – 2,3-butanediol, polyols – glycerol; sugar alcohols – arabitol, mannitol
saccharides	glucose, fructose, arabinose, rhamnose, xylose, glucosan, pectin, gum
acids	volatile – acetic, formic, butyric, propionic acid; fixed – tartaric, malic, lactic, citric, isocitric, fumaric, α-ketoglutaric, succinic acid
phenols and related phenol (phenyl) derivatives	flavonoids – flavonol, catechin, anthocyanin, leucoanthocyanin; non-flavonoids – tartaric acid ester of caffeic, p-coumaric, ferulic acid
aldehydes	acetaldehyde, hexanal, hexenal, furfural, cinnamaldehyde
ketones	β-damascenone, α-ionone, β-ionone
acetals	5-hydroxy-2-methyl-1,3-dioxane, 4-hydroxymethyl-2-methyl-1,3-dioxolane
esters	ethyl acetate, isoamyl acetate, ethyl butyrate, lactones – 2-vinyl-2-methyltetrahydrofuran-5-one, 2-pentenoic acid-γ-lactone
terpenes	linalool, α-terpineol
N-containing compounds	inorganic – ammonia, nitrates; organic – amines, amides, amino acids, pyrazines, nitrogen bases
S-containing compounds	inorganic – sulfites; organic – amino acids (cysteine, methionine)
macromolecules	carbohydrates, proteins, nucleic acids, lipids
vitamins	C, B_1, B_2
metals	see section 3.1 Metals in wine, their role and origin

Tab. 2: Role of particular metals in wine-making process (Pohl, 2007).

Metal	Role in wine-making process
K, Ca	regulation of yeast metabolism by maintaining adequate pH and ionic balance; affecting wine conservation through enhancement of oxidation and clouding effect of Cu and Fe
Mg, Na	regulation of yeast metabolism by maintaining adequate pH and ionic balance
Cu, Fe, Mn	required for prosthetic metallo-enzyme activation; changes in stability of old wine; modification of sensory quality; determination of ageing characteristics, final aroma, taste and color of wine; together with organic chelating ligands is an important natural anti-oxidative mechanism preventing staleness and spoilage of wine
Fe	catalyst of oxidation of polyphenolic substances
Mn	catalyst of acetaldehyde formation
Zn	required for prosthetic metallo-enzyme activation

such as bentonites, used for purification of wines from tarnishing components can be a source of Na, Ca or Al. Increased Ca concentration may be also the result of the use of $CaCO_3$ for de-acidification of wine (Kment, 2005; Pohl, 2007).

Therefore, the analysis of elemental composition of wine is of high importance when considering the risk of excessive intake of toxic metals (Al, As, Cd, Cr, Pb, etc.) potentially present in wine. Another aspect is the wine-making and quality assurance of branded wines, which is of economic importance. Regarding the differences in the elemental composition of soil and applied wine-making procedures (application of substances such as fertilizers, pesticides, fungicides, fining and clarifying substances, choice of materials that wine comes into contact with during the wine-making process) creates conditions to apply the elemental analysis to the identification of wines according to their origin and/or applied wine-making procedure. Knowing of elemental composition of wines may help the wine producers to take measures to increase the quality of their products.

3.2 Analytical methods for elemental analysis of wine

Several methods for elemental analysis of wine samples, such as atomic absorption spectroscopy (AAS), types of which are electrothermal (ETAAS) and flame atomic absorption spectroscopy (FAAS), total reflection X-ray fluorescence (TXRF) and in-

ductively coupled plasma optical emission spectroscopy (ICP-OES) and mass spectrometry (ICP-MS) have been introduced up till now. We provide a short summary of detected elements and their *LOD*s in Tab. 3. However, no mention about the elemental analysis of wine samples by LIBS has been found up till now.

Wine is a complex matrix (see Tab. 1), and thus the above-mentioned techniques are often used after the initial sample pretreatment, that is applied in order to decompose wine and avoid possible matrix interferences. Moreno et al. (2008) tested three preliminary sample treatment methods (dry ashing, wet ashing and alcohol removing technique) for wine analysis by ICP-OES. They evaluated the dry ashing sample pretreatment technique to be the most suitable for elemental analysis of wine by ICP-OES. Tab. 3 also indicates the amount of wine used for elemental analysis and whether any sample pretreatment was employed or not. Except one case, i.e. Gruber et al. (2006), sample pretreatment method was always applied. The most of the authors used for wine decomposition one or more of the following reagents: HNO_3, HCl, H_2SO_4, H_2O_2, distilled water, etc., in a complex procedure consisting of several steps often lasting for long hours, e.g. dry ashing technique applied by Moreno et al. (2008) lasting for more than $48\,h$.

Except routine elemental analysis of wine samples, several studies have been done providing the classification of wines according to their metal content, i.e. Frías et al. (2003), Jos et al. (2004), Galgano et al. (2008), Serapinas et al. (2008), Šelih et al. (2014), etc. Some authors even tried to classify wines considering the results of the elemental analysis of soil, e.g. Kment et al. (2005). As the differentiation of wines is not possible just by simple comparison of the results of their elemental analysis, various statistical techniques, such as analysis of variance (ANOVA; Frías et al. (2003), Galgano et al. (2008), Serapinas et al. (2008)), as well as chemometric methods, such as principal component analysis (PCA; Frías et al. (2003), Kment et al. (2005), Serapinas et al. (2008)), cluster analysis (CA; Frías et al. (2003), Kment et al. (2005)), linear discriminant analysis (LDA; Frías et al. (2003), Jos et al. (2004), Moreno et al. (2007)), soft independent modelling of class analogy (SIMCA; Frías et al. (2003), Jos et al. (2004)), artificial neural networks (ANN; Moreno et al. (2007), Šelih et al. (2014)) were applied.

Tab. 3: Elemental analysis of wines by absorption and emission spectroscopy, X-ray fluorescence spectroscopy and mass spectrometry; V is the volume of sample used and SP refers to the need of sample pretreatment, na - not available.

Analytical method	**Detected element (*LOD [µg/l]*)**	***V [ml]***	**SP**	**References**
ETAAS	*Al* (3), *As* (0.5), *Cd* (0.25), *Pb* (1)	10	✓	Galani-Nikolakaki et al. (2002)
AAS	*Ca* (*na*), *Fe* (*na*), *K* (*na*), *Mg* (*na*), *Mn* (*na*), *Na* (*na*)	50	✓	Kment et al. (2005)
AAS	*Ca* (60), *Fe* (4), *K* (5), *Mg* (10), *Mn* (0.1), *Na* (2), *Zn* (0.45)	10	✓	Galgano et al. (2008)
ETAAS	*Cd* (0.03), *Pb* (0.8)	0.5 - 5	✓	Freschi et al. (2001)
ETAAS	*Tl* (0.05)	50	✓	Cvetković et al. (2002)
ETAAS	*Cd* (0.008)	5	✓	Lara et al. (2005)
ETAAS	*As* (5), *Cd* (0.03), *Cu* (1.2), *Pb* (0.8)	2.5 - 5	✓	Ajtony et al. (2008)
ETAAS	*Pb* (0.29)	20	✓	Dessuy et al. (2008)
FAAS	*Fe* (0.22)	na	✓	Ferreira et al. (2007)
FAAS	*Fe* (12), *Mn* (8)	10	✓	Ferreira et al. (2008)
FAAS	*Cd* (1.8), *Cu* (12.9), *Pb* (5.3)	na	✓	Schiavo et al. (2008)
FAAS	*Fe* (30), *Mn* (22)	5	✓	Dos Santos et al. (2009)
FAAS	*Mn* (0.007)	150	✓	Pohl (2009)
FAAS	*Fe* (10)	150	✓	Pohl et al. (2009)
FAAS	*Cu* (6.3), *Fe* (2.4)	2	✓	Seeger et al. (2015)
ICP-OES	*Al* (0.08), *Ba* (0.02), *Be* (0.1), *Ca* (0.13), *Ce* (0.1), *Cd* (0.1), *Co* (0.01), *Cr* (0.11), *Cu* (0.4), *Dy* (0.1), *Er* (0.1), *Eu* (0.1), *Fe* (0.07), *Gd* (0.1), *Ho* (0.1), *K* (0.12), *La* (0.1), *Li* (0.07), *Lu* (0.1), *Mg* (0.1), *Mn* (0.03), *Mo* (0.1), *Na* (0.12), *Nd* (0.1), *Ni* (0.1), *Pb* (11), *Pr* (0.1), *Sc* (0.05), *Se* (6), *Sm* (0.1), *Sr* (0.03), *Tb* (0.1), *Ti* (0.09), *Tm* (0.1), *V* (0.05), *Y* (0.1), *Yb* (0.1), *Zn* (0.07)	2	✓	Gonzálves et al. (2009)
ICP-OES	*Al* (13), *B* (11), *Ca* (14), *Cu* (10), *Fe* (9), *K* (62), *Mg* (27), *Mn* (8), *Na* (40), *Zn* (6)	na	✓	Šelih et al. (2014)
USN-ICP-OES	*Al* (0.3), *Ca* (0.02), *Cr* (0.2), *Cu* (0.04), *Fe* (0.2), *Ni* (5), *Pb* (0.28), *Zn* (0.1)	5	✓	Lara et al. (2005)
TXRF	*Cr* (10), *Cu* (10), *Fe* (10), *Mn* (10), *Ni* (10), *Zn* (10)	10	✓	Galani-Nikolakaki et al. (2002)
TXRF	*Ca* (*na*), *Cu* (37), *Fe* (*na*), *K* (*na*), *Mn* (*na*), *Rb* (*na*), *Sr* (*na*)	1.2	×	Gruber et al. (2006)
ICP-MS	*Ag* (0.01), *Al* (2), *As* (0.05), *Ba* (0.02), *Be* (0.1), *Cd* (0.05), *Co* (0.02), *Cr* (0.2), *Cs* (0.03), *Cu* (0.5), *Li* (5), *Ni* (0.3), *Pb* (0.1), *Rb* (0.05), *Sb* (0.07), *Sr* (0.01), *Tl* (0.02), *U* (0.07), *V* (0.02), *Zn* (0.5)	50	✓	Kment et al. (2005)
ICP-MS	*Ag* (0.08), *Al* (1.43), *As* (0.02), *B* (14), *Ba* (0.03), *Be* (0.002), *Bi* (0.008), *Br* (34.1), *Cd* (0.008), *Co* (0.006), *Cr* (0.024), *Cs* (0.002), *Cu* (0.021), *Ga* (0.025), *Ge* (0.011), *I* (0.021), *In* (0.002), *Li* (0.022), *Mo* (0.058), *Nb* (0.007), *Ni* (0.08), *P* (11), *Pb* (0.005), *Rb* (0.006), *S* (3538), *Sb* (0.109), *Sc* (0.66), *Se* (0.017), *Si* (475), *Sn* (0.198), *Sr* (0.057), *Te* (0.031), *Th* (0.002), *Ti* (0.07), *Tl* (0.001), *U* (0.001), *V* (0.160), *W* (0.029), *Y* (0.001), *Zr* (0.002)	10	✓	Galgano et al. (2008)
ICP-MS	$^{*}LOD$ $[ng/g]$: *Al* (0.02), *As* (0.05), *B* (0.01), *Ba* (0.001), *Be* (0.01), *Ca* (0.03), *Co* (0.002), *Cr* (0.01), *Cu* (0.01), *Fe* (0.002), *Ga* (0.01), *K* (0.05), *Li* (0.01), *Mg* (0.01), *Mn* (0.01), *Na* (0.01), *Ni* (0.01), *Rb* (0.001), *Sr* (0.001), *Tl* (0.001), *U* (0.005), *V* (0.003), *Zn* (0.01)	na	✓	Serapinas et al. (2008)
ICP-MS	*Cd* (0.0198), *Pb* (0.0104)	2	✓	Cheng et al. (2012)
ICP-MS	*Ag* (1), *As* (3), *Au* (0.6), *Ba* (1), *Be* (1), *Bi* (0.8), *Ce* (0.8), *Co* (0.7), *Cr* (1), *Dy* (0.9), *Ga* (1.2), *Gd* (0.9), *Ge* (2.9), *Hg* (1.3), *Ir* (0.6), *La* (1), *Li* (0.8), *Mo* (0.9), *Nb* (1.4), *Nd* (1.2), *Ni* (1), *Os* (1.5), *Pb* (0.6), *Pd* (1.5), *Pt* (0.35), *Re* (1.4), *Ru* (0.8), *Sb* (0.8), *Sc* (1.5), *Se* (2), *Sn* (1.3), *Ta* (0.8), *Ti* (5), *V* (0.7), *W* (0.4), *Y* (1.3), *Zr* (1.1)	na	✓	Šelih et al. (2014)

4 Experimental part

4.1 Sample preparation

For the study of Sr content in wine samples, SCS4 set of calibration standards in the concentration range from $0\,mg/l$ to about $30\,mg/l$ (see Tab. 4) and a validation sample with concentration $2.96\,mg/l$ were prepared by dilution of $SrCl_2.6H_2O$ (Merck KGaA) in a commercially available red wine (S4) from Slovakia. Six other wine samples obtained directly from wine-growers from four different regions in Slovakia were studied as well. Samples were stored in sterile plastic containers in refrigerator at $5\,^{\circ}C$. Just before measurements, samples were kept outside for at least $30\,min$ in order to stabilize their temperature with the temperature in the room ($20 \pm 1.5\,^{\circ}C$).

Wine samples were studied on two types of targets, i.e. aluminium targets (Al 99.50%, Si 0.25%, Fe 0.40%, Cu 0.05%, Mn 0.01%, Cr 0.01%, Zn 0.07%, Ti 0.05% and the rest consisted of common impurities not further specified; surface area $5 \times 5\,cm$; Metal Service Centre – IMC Slovakia, s.r.o.) and pure silicon targets (n-type silicon substrates prepared by Czochralski method using phosphorus with resistivity of $5-15\,\Omega cm$; surface area $5 \times 5\,cm$; St. Peters, USA). Both, aluminium and silicon targets, were analysed to determine their purity. Aluminium targets were first polished by using sandpaper (Imperial P 600), then cleaned with acetone (Centralchem, s.r.o.) in ultrasonic cleaner (Digital Ultrasonic Cleaner PS-10A) for $10\,min$, after that 3-times washed with pure acetone and 3-times with deionised water. Despite the complex cleaning procedure, the aluminium targets still contained significant amounts of Ca, Mg, Na and K, and thus were not used for the study of elemental composition of wines with different origin, only for the analysis of wine samples doped with known amounts of Sr. On the other hand, we did not detect any of the above-mentioned elements in silicon targets, thus they could be used for both types of analysis. Each wine sample was applied to a new aluminium or silicon target in order to avoid any contamination.

The sample preparation procedure itself consisted in dropping $2\,ml$ of a sample on a target by using a micropipette with maximum volume of $1\,ml$. Prior to the application of a sample to a target (either aluminium or silicon), the sample was being mixed for $1\,min$ and the target was cleaned according to the above-mentioned procedures. The sample was homogeneously dried on a target by using an infrared lamp (Unitra) placed approximately $5.5\,cm$ above the target surface. The drying process lasted for $30\,min$ and then, the sample was kept for approximately $6\,min$ to stabilize its temperature before laser ablation.

4.2 Experimental setup

The experimental setup, the scheme of which is depicted in Fig. 5 has been built for wine sample analysis in LIBS laboratory at FMFI UK, Bratislava, Slovakia. A Q-switched Nd-YAG laser (CFR, QUANTEL) operating at $266\,nm$ (4-th harmonic) with repetition rate of $10\,Hz$ was used for plasma generation. $80\,mJ$ laser pulses had duration of $8\,ns$.

Mirrors MR1, MR2 and MR3 (Nd:YAG Laser Mirror, 4-th Harmonic, Thorlabs, $> 99\%$) were used to control the path of laser pulses. Laser pulses were focused by lens LN1 (UV Fused Silica Plano-Convex Lens, Thorlabs, focal length $175\,mm$) slightly below the sample surface. $Hg-Ar$-lamp (Ocean Optics, Hg-1) was used to check the position of laser light incidence on the surface of a target as well as to check if lens LN2 (focal length $75\,mm$, Thorlabs) was properly fixed to collect plasma emission into optical fibre (Ocean Optics). The optical fibre was, in turn, connected to echelle spectrometer (Mechelle ME 5000, Andor Technology) equipped with ICCD camera (iStar, DH734i-18F-03). Spectral range of the spectrometer was $230-850\,nm$ and its resolving power $\frac{\lambda}{\Delta\lambda} = 5000$. Targets with wine samples were placed on translation stage S. It was possible to change its x, y and z positions manually by turning screw adjusters.

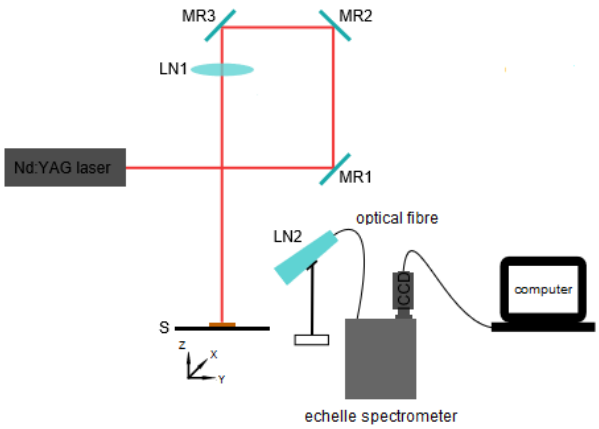

Fig. 5: Scheme of LIBS experimental setup.

Tab. 4: Concentrations of Sr (c_{Sr}) in SCS4 set of calibration standards (CS).

No. of CS	1	2	3	4	5	6	7	8
c_{Sr} [mg/l]	0	0.522	5	10	15.034	20	25	30.068

4.3 Measurement procedure

Measurements were performed at atmospheric pressure and at room temperature of $20 \pm 1.5\ ^{\circ}C$.

First, optimal parameters for our measurements were found. Aluminium and silicon targets have diverse qualities (such as reflectivity, elemental composition, etc.), thus the optimal parameters for measurements using aluminium targets slightly varied from the optimal parameters for measurements using silicon targets. SNRs were studied to choose the best GDs, GWs and vertical stage positions. We used $300\,ns$ GD for measurements with aluminium targets and $400\,ns$ GD for those with silicon targets. GW and gain of the ICCD camera were set the same in both cases, i.e. $3\,\mu s$ and 180, respectively. The vertical position of the translational stage with respect to the focusing lens LN1 was examined for both targets separately, as they had different thicknesses.

For each sample, six spectra of 150 single shots were taken. In order to take each single shot at an untouched spot, the position of the stage with a target was being manually changed with a screw adjuster after every single shot. 50 single shots were taken in approximately $3\,cm$ long line along x-axis, then the stage was shifted $3\,mm$ along y-axis and another 50 single shots were taken in the same way. In this way, virtually most of the target area was scanned.

In Fig. 6, we can see course of a measurement of the red wine sample S4. There are weak light bands on the left side of the target, which are, actually, the craters after laser ablations. There are some more intense dots that are caused by focusing the laser pulses closer to each other, which was common at the end position of the stage in the x-axis. The lens in the upper left part of the picture is the L1 lens, which is used to focus laser pulses on the target. In the upper right side, we can see the holder with the L2 lens, which is used to collect light from plasma emission. The distance between the focusing optics and the target surface was more than $170\,mm$, thus no shielding to protect lenses from splashes was needed.

4.4 Results

First calibration curves of Sr in SCS4 set of calibration standards applied to aluminium as well as silicon targets were established. Calibration curves may be, in general, established as linear fit of spectral line intensities. We can describe them by the following equation

$$y = a + bx \tag{3}$$

where y refers to the spectral line intensity of the studied element, x to the concentration of the element, and a is the intercept and b the slope of the calibration curve. Coefficients of determination R^2, indicating how well our experimental data fit established calibration curves, were determined as well (see Fig. 9. In Fig. 10).

Calibration curves actually relate the spectral line intensity of an element in the plasma to the concentration of the element in the sample. However, spectral line intensity of the element in the plasma is related to the ablated mass of the sample, which is, in turn, related to the laser radiation parameters, such as laser energy and focusing of the laser on the sample. Moreover, the laser plasma characteristics, such as variations of plasma temperature and its interaction with the sample surface also influence the emission signal. Thus, the analytical precision and consequently accuracy may be influenced by either systematic or random changes in the above-mentioned parameters (Zorov, 2010).

Therefore, in order to reduce the influence of the above-mentioned phenomena on the linearity of calibration curves, normalization of Sr spectral lines was performed. Ca spectral lines were chosen as reference lines for normalization due to the relatively high amount of Ca present in wine samples, which was thus expected to substantially influence plasma properties.

Individual lines for normalization were selected with respect to the thermodynamic criterion described by Zorov et al. (2010). To overcome the influence of electronic density on the ratio of line intensities, the same ionisation stage of the reference line for normalization was chosen as is the ionisation stage of the analysed element, i.e. $Sr\ II$ ionic lines

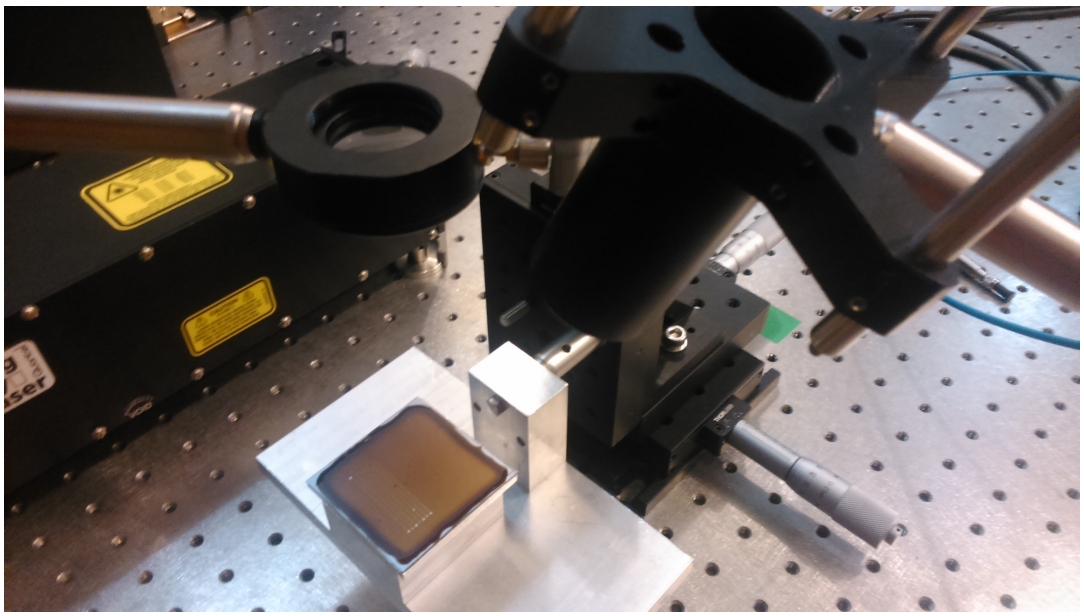

Fig. 6: Course of a measurement of the red wine sample S4 on the silicon target (FMFI UK, Bratislava, Slovakia).

were normalized by ionic line $CaII$ and $Sr\ I$ neutral lines by neutral line CaI. In order to neglect the influence of plasma temperature on ratio of line intensities, we tried to pick out such $CaII$ and CaI lines that have their upper energy states close to the upper energy states of $SrII$ and SrI lines, respectively.

Calibration curves were used to calculate *LOD*s according to the 3σ-criterion defined by the International Union of Pure and Applied Chemistry (IUPAC)

$$LOD = \frac{3\sigma}{b} \tag{4}$$

where σ is the standard deviation of the experimental spectrum and b is the slope of the calibration curve. This formula defines *LOD* as the smallest concentration that can be detected with a confidence level of about 90% (Thomsen, 2003).

*LOD*s of a particular element are determined by intensities of its emission lines, which are, in turn, determined by their excitation energies and transition probabilities (Einstein coefficients) together with plasma properties (temperature and electron density). Thus different elements will have different *LOD*s.

In Fig. 7, we can see part of the spectrum of CS8 (concentration of Sr $c_{Sr} = 30.068\,mg/l$) calibration standard of SCS4 set on silicon target showing the most intense Sr lines, i.e. $SrII$ (407.771 nm and 421.552 nm) and SrI (460.733 nm; 472.228 nm; 478.432 nm; 481.188 nm and 483.204 nm) and in Fig. 8 detail of the $SrII$ (421.552 nm) line of CS2 (concentration of Sr $c_{Sr} = 0.522\,mg/l$) calibration standard of SCS4 set on silicon target. Two most intense spectral lines of $SrII$ (407.771 nm and 421.552 nm) as well as two spectral lines of SrI (460.733 nm and 481.188 nm) were used to plot calibration curves (see Fig. 9 and Fig. 10). Individual points represent average intensities of replicate spectra of calibration standards and the error bars their standard deviations (*SD*s).

We can see that spectral intensities of calibration standards in Fig. 9 b) and d), and Fig. 10 a) and b) can be described by polynomial function rather than by the linear one (see Eq. 3). Therefore, the data are fitted by the polynomial function

$$y = a + bx - cx^2 \tag{5}$$

where y refers to the spectral line intensity of the studied element, x to the concentration of the element, a is the intercept and $\frac{c}{b}$ measures the non-linearity of the calibration curve. If $c = 0$, Eq. 5 is transformed into Eq. 3, which corresponds to the linear calibration curve. *LOD*s for the polynomial calibration curves were calculated by fitting the linear part of the calibration curves by a tanget at the point $x = 0$, which virtually means that the slope of the calibration curve b in Eq. 4 is then equal to the parameter b in Eq. 5.

Respective values of coefficients of determination R^2, limits of detection *LOD*s and parameters a, b

and c of calibration curves from Eq. 3 and Eq. 5 are mentioned in Tab. 5 and Tab. 6.

Afterwards, the validation sample with Sr concentration of $2.96 mg/l$ in S4 wine was used to validate the accuracy of established calibration curves in Fig. 9 and Fig. 10. Actually, all of the Sr concentrations mentioned in the experimental part of the work are meant as concentrations of Sr added to wine samples, not considering their concentrations already present in them. In Fig. 11, we can see the results of the validation, where individual points refer to the concentration values calculated from calibration curves and error bars to their standard deviations; $c_{nominal}$ refers to the nominal concentration of $2.96 mg/l$, $c_{average}$ to the average concentration calculated from all individual points, and c_{max} and c_{min} to $c_{average} \pm SD$ of average concentrations, respectively.

Finally, the elemental composition of six wine samples obtained directly from wine-growers from four different wine-growing regions (R1 – R4) in Slovakia was determined (see Tab. 7). Elements, such as C, H, O and N are not of our interest as all of the measurements were carried out in air atmosphere. Si lines were also not studied, as Si was the main constituent of the matrix used for elemental analysis. In Fig. 12, we can compare the elemental composition of white wine (Ww) samples. In Fig. 13, the elemental composition of white (Ww) and red wine (Wr) from the same wine-growing region is shown.

Precision performance of the new sample preparation method was evaluated by plotting the RSD of normalized intensities of Sr lines against their concentration in wines (see Fig. 14).

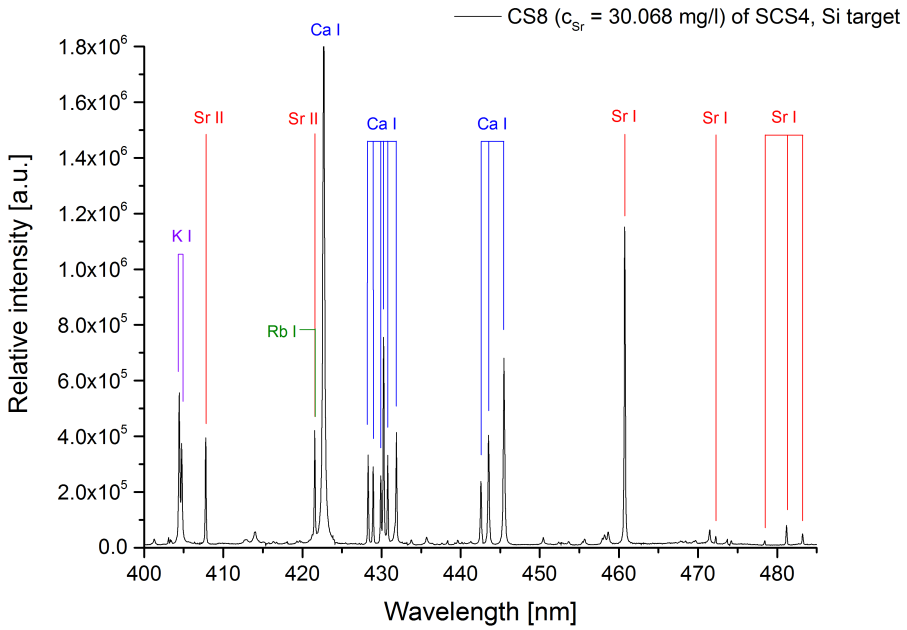

Fig. 7: Part of the spectrum of CS8 ($c_{Sr} = 30.068\,mg/l$) calibration standard of SCS4 set on silicon target showing the most intense Sr lines, i.e. $SrII$ (407.771 nm and 421.552 nm) and SrI (460.733 nm; 472.228 nm; 478.432 nm; 481.188 nm and 483.204 nm).

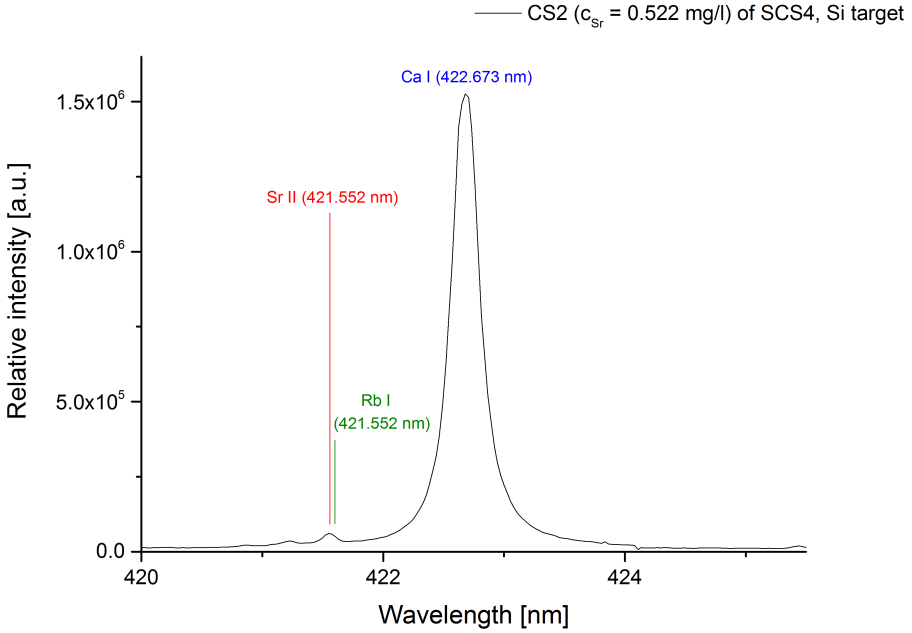

Fig. 8: $SrII$ (421.552 nm) spectral line in the spectrum of CS2 ($c_{Sr} = 0.522\,mg/l$) calibration standard of SCS4 set on silicon target.

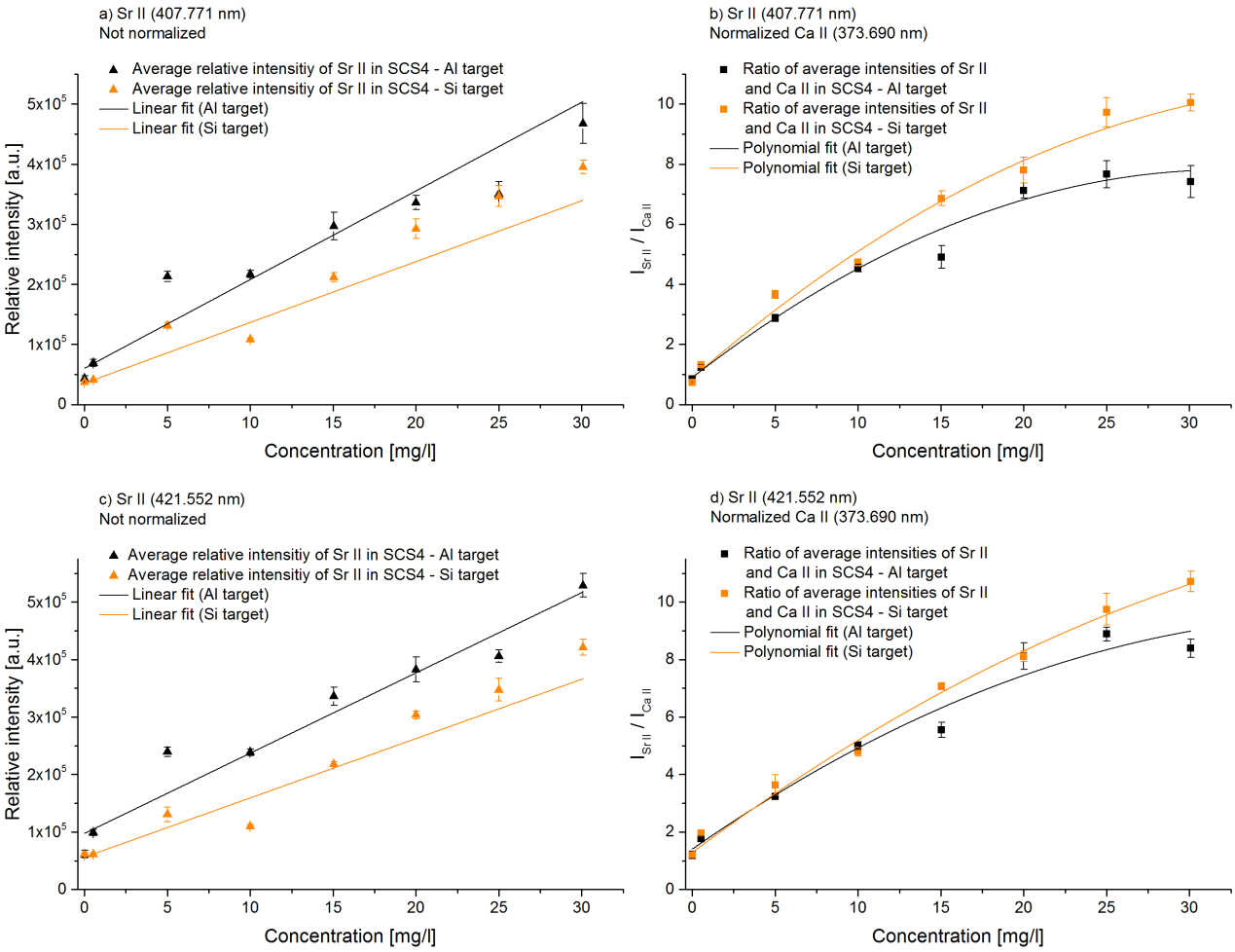

Fig. 9: Calibration curves of $SrII$ in SCS4 set of calibration standards using aluminium (black) and silicon (orange) targets; a) and b) $SrII$ (407.771 nm), and c) and d) $SrII$ (421.552 nm) without and with normalization by $CaII$ (373.690 nm), respectively; I_{SrII} is the relative intensity of $SrII$ and I_{CaII} is the relative intensity of $CaII$.

Tab. 5: Parameters (coefficients of determination R^2, limits of detection LODs, parameters a, b and c from Eq. 3 and Eq. 5) describing calibration curves of $Sr\ II$ in SCS4 in Fig. 9; NA - not applicable.

	***SrII* (407.771 *nm*), not normalized**		***SrII* (407.771 *nm*), normalized *CaII* (373.690 *nm*)**		***SrII* (421.552 *nm*), not normalized**		***SrII* (421.552 *nm*), normalized *CaII* (373.690 *nm*)**	
Paramater	**Al target**	**Si target**	**Al target**	**Si target**	**Al target**	**Si target**	**Al target**	**Si target**
R^2	0.8977	0.8867	0.9903	0.9745	0.9041	0.9059	0.9789	0.9850
LOD [mg/l]	0.485	0.603	0.260	0.291	NA	NA	NA	NA
a [a.u.]	60485.82	35389.90	0.90	0.89	97575.23	56063.92	1.41	1.29
$b\ [\frac{a.u.}{mg/l}]$	14756.35	10124.59	0.43	0.48	13964.93	10323.34	0.40	0.43
$c\ [\frac{a.u.}{(mg/l)^2}]$	NA	NA	0.01	0.01	NA	NA	0.005	0.004

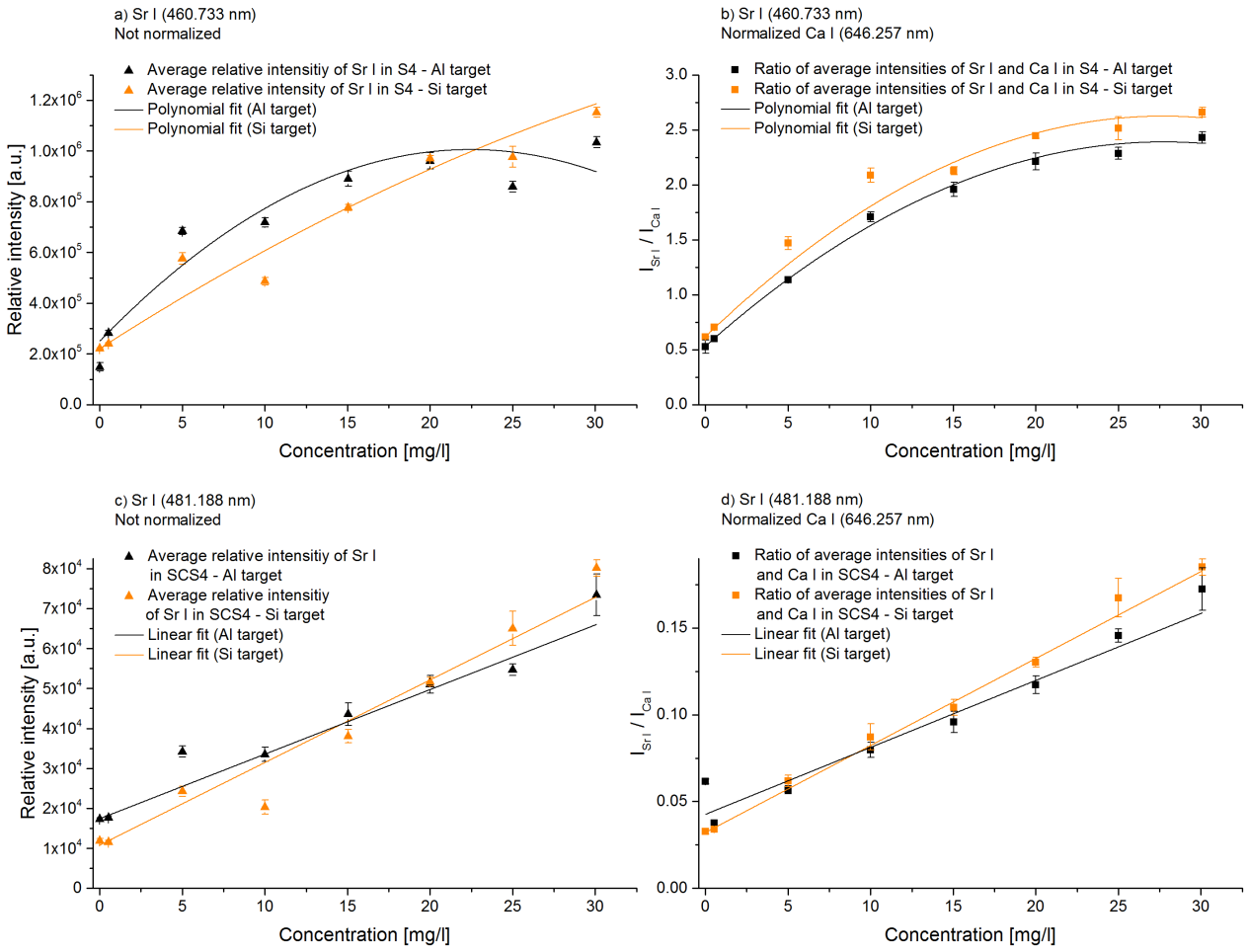

Fig. 10: Calibration curves of SrI in SCS4 set of calibration standards using aluminium (black) and silicon (orange) targets; a) and b) SrI (460.733 nm), and c) and d) SrI (481.188 nm) without and with normalization by CaI (646.257 nm), respectively; I_{SrI} is the relative intensity of SrI and I_{CaI} is the relative intensity of CaI.

Tab. 6: Parameters (coefficients of determination R^2, limits of detection LODs, parameters a, b and c from Eq. 3 and Eq. 5) describing calibration curves of $Sr\ I$ in SCS4 in Fig. 10; NA - not applicable.

	***SrI* (460.733 *nm*), not normalized**		***SrI* (460.733 *nm*), normalized *CaI* (646.257 *nm*)**		***SrI* (481.188 *nm*), not normalized**		***SrI* (481.188 *nm*), normalized *CaI* (646.257 *nm*)**	
Paramater	**Al target**	**Si target**	**Al target**	**Si target**	**Al target**	**Si target**	**Al target**	**Si target**
R^2	0.8786	0.9799	0.9956	0.9939	0.9528	0.9685	0.7720	0.9973
LOD [mg/l]	0.277	0.232	0.207	0.053	3.586	2.124	4.146	0.747
a [a.u.]	250831.97	221154.52	0.53	0.62	17398.85	10820.66	0.04	0.03
$b\ [\frac{a.u.}{mg/l}]$	67300.16	41857.40	0.13	0.14	1616.66	2066.48	0.004	0.005
$c\ [\frac{a.u.}{(mg/l)^2}]$	1500.52	324.19	0.002	0.003	NA	NA	NA	NA

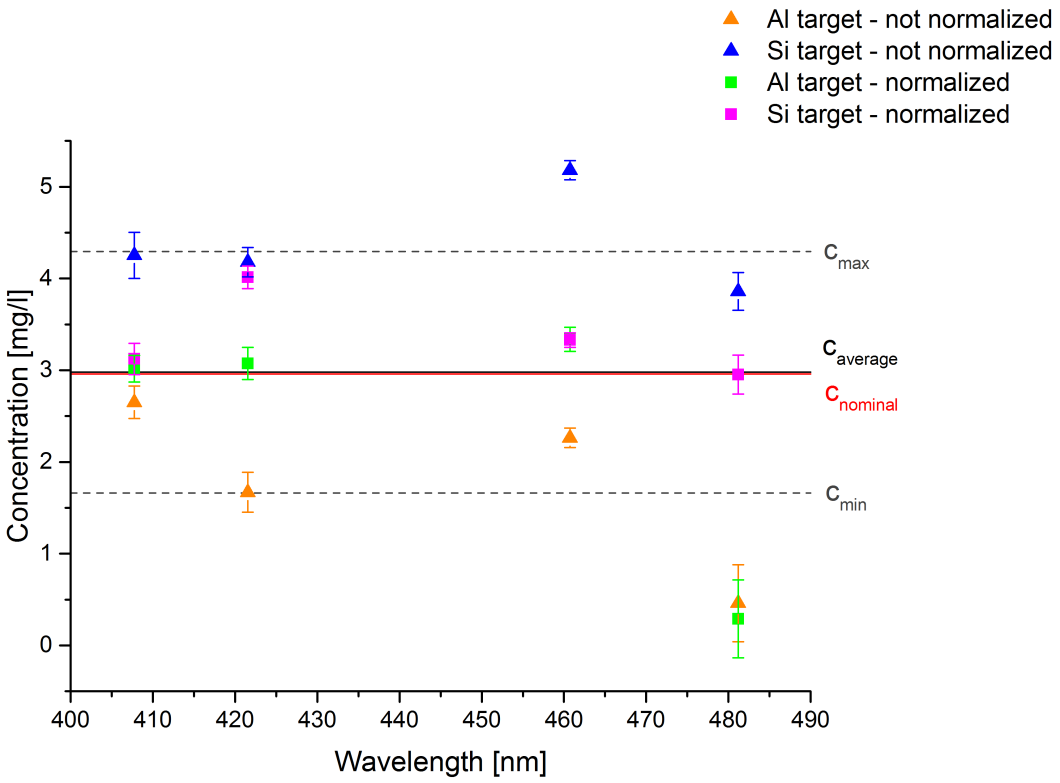

Fig. 11: Validation of calibration curves from Fig. 9 and Fig. 10, $c_{nominal}$ is the nominal concentration of $2.96 mg/l$, $c_{average}$ is the average concentration calculated from all individual points, and c_{max} and c_{min} are $c_{average} \pm SD$ of average concentrations, respectively.

Tab. 7: List of elements and corresponding characteristic spectral lines detected in Slovak wine samples on silicon targets.

Detected element	**Species**	**Wavelength *[nm]***
Al	*Al I*	394.401
Ca	*Ca I*	612.222
Fe	*Fe I*	344.061 / 344.099
K	*K I*	691.108
Li	*Li I*	670.776 / 670.791
Mg	*Mg II*	517.268
Mn	*Mn I*	403.076
Na	*Na I*	589.592
Rb	*Rb I*	780.027
Sr	*Sr I*	460.733

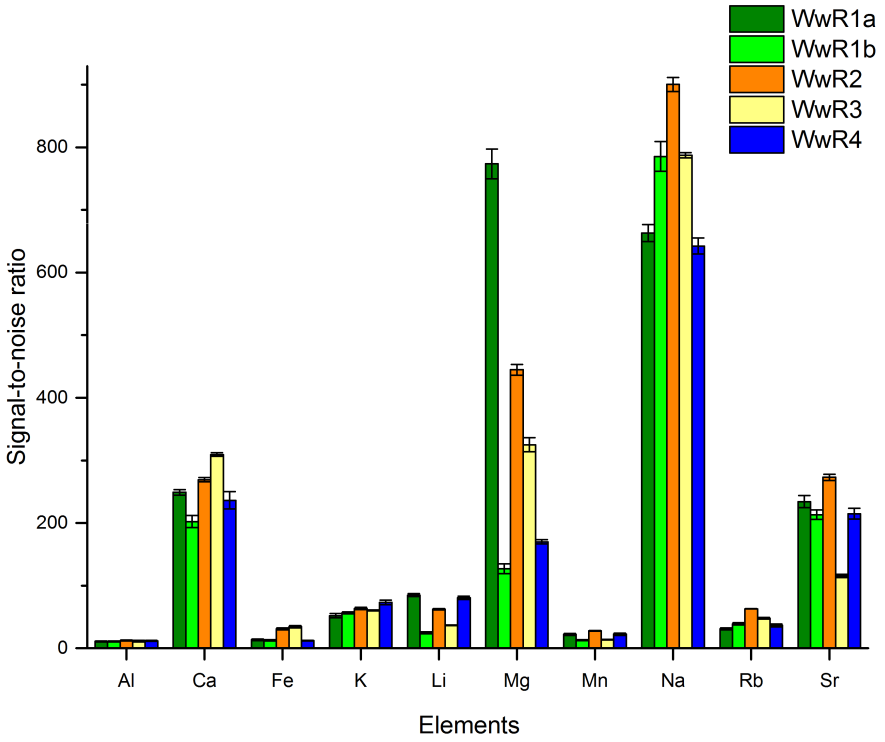

Fig. 12: Comparison of the elemental composition of Slovak white wines (Ww) from four different regions (R1 – R4), wines WwR1a and WwR1b are from the same region produced by two different producers; silicon target.

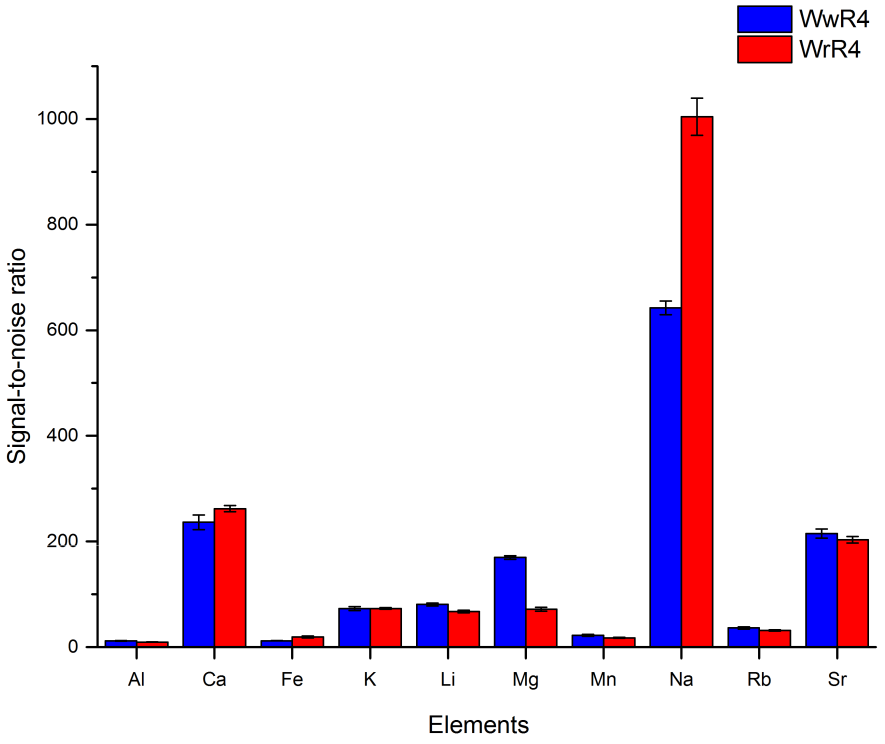

Fig. 13: Comparison of the elemental composition of white (WwR4) and red wine (WrR4) from R4 region in Slovakia; silicon target.

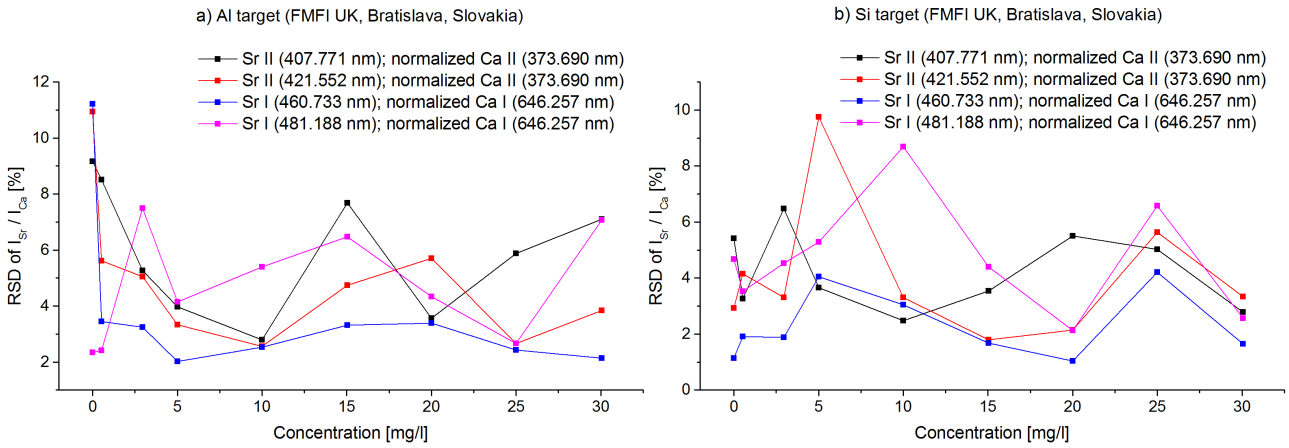

Fig. 14: Precision performances of measurements using SCS4 set of calibration standards and validation sample with nominal concentration of Sr $c_{Sr} = 2.96 mg/l$ on a) aluminium and b) silicon targets at FMFI UK, Bratislava, Slovakia; I_{Sr} and I_{Ca} are the relative intensities of Sr and Ca, respectively.

4.5 Discussion

First, wine samples with known amounts of *Sr* were studied on aluminium as well as silicon targets. Aluminium and silicon have much different behaviour at 266 *nm* wavelength. While laser beam of 266 *nm* wavelength is reflected by aluminium targets, silicon targets strongly absorb in ultraviolet (UV) region.

In Fig. 7, we can see the most suitable *Sr* lines that were considered to be used for plotting calibration curves. In order to reach the lowest possible *LOD*s, three most intense lines *Sr II* (407.771 *nm* and 421.552 *nm*) and *Sr I* (460.733 *nm*) were chosen to plot calibration curves (see Fig. 9 and Fig. 10). Calibration curves of *Sr II* in Fig. 9 a) and c) show fluctuations around linear fit, however, just after normalization by *Ca II* (373.690 *nm*) line, it is clear that the calibration curves exhibit polynomial trend (see Fig. 9 b) and d)). Polynomial trend of the calibration curve may be also observed for *Sr I* (460.733 *nm*) line (see Fig. 10 a) and b)). It is induced by self-absorption effect at higher concentrations of *Sr*. After detailed study, we uncovered that *Sr II* (421.552 *nm*) line (see Fig. 8) is in general not suitable for the determination of *Sr* concentration as it interferes with *Rb I* (421.552 *nm*) resonant line. In our experiments, the calibration curves of *Sr* were built by using just one type of wine with constant *Rb* content, so the possible influence of *Rb* on the intensity of *Sr II* (421.552 *nm*) line was also constant. However, for different wines, the *Rb* content may vary, which may introduce uncertainties into emission intensities of *Sr II* (421.552 *nm*) line. This line also lies close to the intense resonant *Ca I* (422.673 *nm*) line, which degrades the possibility to use *Sr II* (421.552 *nm*) line for the identification of small concentrations of *Sr*. Therefore, *Sr II* (421.552 *nm*) line was not used for the determination of *LOD*s. The only line that did not suffer from self-absorption is *Sr I* (481.188 *nm*). Its calibration curves before and after normalization by *Ca I* (646.257 *nm*) line are in Fig. 10 c) and d)).

In all of the cases, except for *Sr I* (481.188 *nm*) on aluminium target, normalization led to higher values of coefficients of determination R^2 (see Tab. 5 and Tab. 6). The intensity of *Sr I* (481.188 *nm*) line is approximately up to an order of magnitude lower than the intensities of other *Sr* lines (see Fig. 7). Therefore at low concentrations, the fluctuations of background strongly influence also the intensity of emission lines. Thus, we can observe an outlying point in Fig. 10 d) belonging to S4 wine sample with *Sr* concentration $c_{Sr} = 0\,mg/l$. Outlying points at the beginning and at the end of calibration curves strongly influence their slope, and thus decrease the values of coefficients of determination R^2. Based on the plots of calibration curves, similar behaviour of calibration curves of *Sr* may be observed for both, aluminium and silicon targets, despite different interaction effects with 266 *nm* laser pulses (already mentioned above). In order to quantitatively assess the difference between aluminium and silicon targets, more experiments need to be performed employing additional elements and plasma parameters need to be studied as well. The lowest value of *LOD*s was achieved for the most intense *Sr I* (460.733 *nm*) line on silicon target, i.e. $0.053\,mg/l$.

Subsequently, the accuracy of calibration curves was tested (see Fig. 11). We have already excluded the suitability of using *Sr II* (421.552 *nm*) line for concentration estimation of *Sr* in different wines. We can see that when using this line even within the same wine samples, the estimated concentrations are deviated from the value of nominal concentration of $2.96\,mg/l$, except for the aluminium target after normalization. In the case of *Sr I* (481.188 *nm*) line, the uncertainties in the concentration estimation are even higher, especially for the aluminium target, which may be partially explained by uncertainties in the estimation of calibration curves due to the outlying data point at the beginning part of the calibration curves. We can see that even standard deviations of six replicate measurements are higher compared to other data points. This is due to the fact that this line is very weak compared to other lines (up to an order of magnitude lower intensity; see Fig. 7) and at low concentrations, there is higher impact of background fluctuations compared to more intense lines. Therefore, *Sr II* (407.771 *nm*) and *Sr I* (460.733 *nm*) lines provide the most accurate calculated concentration values after normalization for both, aluminium and silicon targets.

The elemental composition of six wines obtained directly from wine-growers from 4 different regions in Slovakia is presented in Tab. 7. The elemental composition was studied only on silicon targets as they proved higher level of purity compared to aluminium targets. We can classify detected metals according to their concentrations in wine as it is stated in section 3.1 Metals in wine, their role and

origin:

1. major metals – K, Ca, Mg and Na,
2. minor metals – Al, Fe, Mn, Rb and Sr,
3. trace metals – Li.

Presence of Si was not determined in Slovak wines because of the target materials that were used. $SrCl_2.6H_2O$ (Merck KGaA) was used for the preparation of calibration standards. However, we did not detect Cl even in the calibration standard of the highest concentration. It means that the plasma temperature was not high enough to excite Cl atoms, which are known for their high values of excitation energies.

Fig. 12 shows SNR of individual elements in Slovak white wines from four different regions. Dark and light green stand for two white wines (WwR1a and WwR1b) from the same region. We can see that the proportion of individual elements varies not only between individual regions, which may be caused by the differences in soil composition, but also varies for the two wines within the same region, which may be due to the differences in applied wine-making procedure (e.g. using fertilizers, pesticides, etc.; various additives such as bentonites for purification, sodium bisulfite for sulphurization to avoid spoilage, etc.; using different materials of wine-making machinery and barrels, etc.). Another aspect is the age of vines, as the older vines are, the deeper their roots grow down, and they draw more groundwater rather than surface water.

In order to determine whether the elemental composition of red wines differs from the elemental composition of white wines, we studied SNR of the elements detected in white and red wine from the same producer in R4 wine-growing region. We can observe the most significant differences in the concentrations of Fe, Mg and Na. Therefore, we consider LIBS to be enough sensitive to be used for finding the differences in the elemental composition of wines. However, when it comes to classification, not only region, but also wine-making procedure and type of wine (white, pink or red) has to be considered.

New sample preparation method for the analysis of liquids with organic background, such as wine, has been developed and applied to the analysis of wine samples. We mentioned the alternative ways of liquid analysis by LIBS that have been developed up till now in section 2.3 Alternative ways of liquid analysis by LIBS. However, no-one has ever studied liquid samples with organic background, such as wine, by LIBS. In Tab. 8 we assess the main advantages and disadvantages of the above-mentioned methods that have been used for the analysis of other types of liquids. It is not really possible to compare analytical performance of our method with the others as they did not deal with organic wine matrix.

Our method actually combines the advantages of liquid-to-solid matrix conversion method as well as liquid layer on solid matrix (see Liquid-to-solid matrix conversion and Liquid layer on solid matrix in section 2.4 Transformation of a liquid sample to a solid or a "quasi-solid" sample), as wine samples were dried on solid targets and the organic residuum with metal content remained on the target in the form of a thin viscous layer. The difference is that we applied larger amount of liquid ($2\,ml$) on the sample surface of around $25\,cm^2$, and thus there was enough space to take six replicate measurements in the homogeneous middle part of the target. In this way, we avoided the negative phenomena related to the so-called "coffee-spot" effect described by Metzinger et al. (2014) and did not need to specially modify the substrate surface as it was applied e.g. by Bae et al. (2015). The homogeneous deposition of wine on the sample surface was ensured just by surface tension of liquid sample. To ensure homogeneity, it was crucial to keep the target precisely in horizontal position.

Fig. 14 a) and b) stands for precision performance evaluation of the applied sample preparation procedure on aluminium and silicon targets, respectively. Due to fluctuations, we almost can not see the typical decreasing tendency of RSD, which, in general, has higher values for lower concentrations and decreases with increasing concentration, and thus increasing value of intensity. This phenomenon was described also by Bae et al. (2015) and is mentioned in Liquid-to-solid matrix conversion in section 2.4 Transformation of a liquid sample to a solid or a "quasi-solid" sample as well. However, we should mention that for Sr lines the RSD values vary only from 1.04% to 11.22%. The lowest values of RSD may be observed for SrI ($460.733\,nm$) line studied on silicon targets, which vary only from 1.04% to 4.21%. This is even less than the RSD values obtained by Bae et al. (2015) for K on laser-patterned silicon wafer, LPSW (see Fig. 4). Thus, SrI ($460.733\,nm$) line after normalization proved to give the lowest values of LODs (of the order of $10^{-2}\,mg/l$), its calibration curve had one

Tab. 8: Assessment of alternative ways of sample preparation methods for liquid analysis by LIBS.

Way of analysis	Main advantages	Main disadvantages
Bulk liquids	no sample preparation	significant decrease of spectral intensity due to plasma quenching
DP-LIBS	no sample preparation	complexity and cost of the system, liquids need to be transparent to the first laser pulse
Surface analysis of static bulk liquids	no sample preparation	splashing causing degradation of optical system
Liquid jets	reduced splashing compared to static liquids	risk of nozzle blockage by suspended particles and requirement of a larger sample volume
Analysis of aerosols and isolated microdroplets	discrete nature of LIBS plasma volume	solvent vaporisation consuming part of laser pulse energy
Substrate absorption	relatively fast sample preparation, possible to apply on-site	substrates often having organic background (wood, cellulose, etc.) including lots of trace elements
Liquid-to-solid matrix conversion	benefits of solid sample analysis by LIBS	inhomogeneous distribution of dried solid deposits
Liquid layer on solid matrix	signal enhancement due to the use of a solid substrate	need to keep the thickness of liquid layer constant

of the highest values of coefficient of determination $R^2 = 0.9939$, proved its abilities in validation test of concentration determination using sample with nominal concentration of *Sr* $c_{nominal} = 2.96\,mg/l$ as well as, in general, exhibited the highest precision performance. All of the above-mentioned facts are in favour of choosing this line to be the most appropriate for determination of *Sr* concentration, especially in the case of the concentrations in the linear part of the calibration curve. For higher *Sr* concentrations (approximately $> 10\,mg/l$), however, self-absorption and consequently non-linear shape of the calibration curve may lead to degraded accuracy of concentration prediction.

To sum up, we can mention the advantages of our sample preparation method for LIBS analysis of liquids with organic background over the other methods already used for liquid analysis by LIBS mentioned in section 2.3 Alternative ways of liquid analysis by LIBS:

1. Relatively simple and fast sample preparation procedure with minimal risk of contamination when using new targets each time.
2. Possible to use targets of high purity (e.g. 99.99%), which allows us to choose substrate according to our analytical preferences with minimal loss of analytical information.
3. No special modification of LIBS setup.
4. Benefits of solid sample analysis by LIBS.
5. Signal enhancement with minimum *LOD*s of *Sr* of the order of $10^{-2}\,mg/l$.
6. Reduced splashing compared to bulk liquid analysis. Residual splashing can be solved either by shielding the focusing optics by microscope glass plate or by lengthening the distance between the focusing optics and the target surface (approximately up to $170\,mm$ in our conditions).
7. Low cost.

On the other hand, the main disadvantage of our sample preparation method is the necessity to keep the thickness of wine residuum layer constant throughout the whole target surface by maintaining it precisely in horizontal position. Differences in thickness and humidity may lead to changed plasma parameters, and thus influence intensities of emission lines.

To compare LIBS with other spectrochemical methods already used for wine analysis (see section 3.2 Analytical methods for elemental analysis of wine), we must consider *LOD*s, time and complexity of sample preparation procedure as well as the amount of sample required for analysis.

The minimum *LOD*s of *Sr* reached by LIBS were of the order of $10^{-2}\,mg/l$, while other methods (see Tab. 3) reached substantially lower minimum *LOD*s of this element, i.e. of the order of $10^{-6}\,mg/l$. However, on the other side, we can see from Tab. 3 that all of these methods (i.e. AAS and its types ETAAS and FAAS, ICP-OES, TXRF and ICP-MS)

often used higher volume of samples and required sample pretreatment procedures sometimes lasting for long hours (see section 3.2 Analytical methods for elemental analysis of wine). Therefore, we see the main application of our method to fast in-situ preliminary analysis of liquid samples, such as wine, as its main advantages over other methods are no sample pretreatment, high rate and simplicity of the analysis as well as possibility to use portable LIBS setups for in-situ analysis. We must point out that such analysis is also environmentally friendly as it does not require any sample pretreatment using chemicals.

Conclusion

The main goal of the work was to develop sample preparation method suitable for the analysis of liquids with organic background by laser-induced breakdown spectroscopy (LIBS). Wine samples were studied in our experiments, however, the method may be applied to other liquids having similar background (e.g. fruit and vegetable juices, syrups, etc.) as well. Complications, such as bubble and shock wave formation, related to the analysis of bulk liquids by LIBS were introduced in section 2.2 Laser-induced cavitation, shock wave formation and plasma stability in bulk liquids. Alternative configurations already applied to avoid these difficulties were mentioned in section 2.3 Alternative ways of liquid analysis by LIBS. In section 3.2 Analytical methods for elemental analysis of wine, other spectrochemical techniques already used for wine analysis and their analytical performance were presented. The motivation to use LIBS for such analysis despite the existence of well-established methods was to increase the rate of the analysis, avoid using chemicals for sample pretreatment and, last but not least, to introduce the experimental setup that can be easily applied to the analysis of samples in solid, liquid and gaseous state in-situ.

The experiments were carried out in two stages. The first stage was realized at ILM, Lyon, France under the supervision of prof. Jin Yu and results of this stage have been already submitted for publication titled "Determination of metal elements in wines using surface-assisted laser-induced breakdown spectroscopy" (Bocková et al., 2016). Here, we presented the second part of the experiments that took place at FMFI UK, Bratislava, Slovakia under the supervision of prof. RNDr. Pavel Veis, CSc.

The sample preparation procedure developed at ILM, Lyon, France based on drying of $2\,ml$ of wine on solid target was applied to the analysis of Slovak wine samples. First, calibration curves of wine samples doped with known amount of *Sr* were studied on aluminium and silicon targets. Although these materials react differently to laser radiation in ultraviolet region, graphical representation of calibration curves did not reveal any significant differences in their behaviour. In order to generalise and quantitatively assess the effect of target material, further experiments studying additional elements and determining plasma parameters are necessary.

In the case of *Sr* resonant lines $SrII$ ($407.771\,nm$ and $421.552\,nm$) and SrI ($460.733\,nm$) we dealt with the problem of self-absorption. In addition, $SrII$ ($421.552\,nm$) line was due to the interference with RbI ($421.552\,nm$) line marked to be not suitable for determination of *Sr* concentration. The next line of highest intensity belonging to the group of non-resonant lines (at the same time not suffering from interference with spectral lines of other elements) was SrI ($481.188\,nm$) line. This line was on the other hand approximately up to an order of magnitude less intense than other *Sr* lines, which resulted in lower accuracy in validation test with sample having nominal concentration of $2.96\,mg/l$. Considering the coefficients of determination of calibration curves, results of the validation test, *LOD*s (of the order of $10^{-2}\,mg/l$) and precision performance evaluation after normalization by *Ca* lines, SrI ($460.733\,nm$) line was chosen to be the most suitable line for concentration determination of *Sr* in wine samples, especially for the linear part of its calibration curve (up to *Sr* concentration of around $10\,mg/l$). For higher concentrations, it may however, suffer from degraded accuracy of concentration determination due to self-absorption.

The elemental analysis of Slovak wines obtained directly from wine-growers coming from four distinct regions in Slovakia revealed the presence of the following elements: *Al*, *Ca*, *Fe*, *K*, *Li*, *Mg*, *Mn*, *Na*, *Rb* and *Sr*. *C*, *H*, *O* and *N* were not of our interest as the measurements were carried out in air atmosphere, as well as *Si* being the main constituent of the applied target material. The elemental analysis proved that LIBS is enough sensitive to uncover differences in the proportion of the detected elements present in different wines. Furthermore, it was revealed that

if we want to classify wines according to their origin, we need to consider not only their origin, but also the wine-making procedure as we found significant differences in the composition of two white wine samples coming from two distinct producers from the same region. In addition, significant differences between white and red wines from the same region were seen in the concentrations of Fe, Mg and Na.

Precision performance evaluation was in favour of using the newly developed method for liquid analysis by LIBS, as the *RSD* values of six replicate measurements of wine samples were in the range only from 1.04% to 11.22% for Sr lines. The *RSD* values obtained for SrI (460.733 nm) line after normalization on silicon target varied only in the range from 1.04% to 4.21%. This is even less than the *RSD* values obtained by Bae et al. (2015) for K on laser-patterned silicon wafer, LPSW (approximately 2% to 6%). Therefore, the repeatability of the method has been proven.

Finally, wine analysis by LIBS has been compared with other methods of liquid analysis by LIBS as well as with other methods of wine analysis (AAS, ICP-OES, TXRF and ICP-MS). The main advantage of our method is fast sample preparation (less than 30 min) with no need of chemicals for organic matrix decomposition, while the main drawback are higher *LOD*s compared to other spectrochemical methods.

Therefore, based on the results of our experiments, we see the major potential use of our method for in-situ analysis of organic liquid samples when no time for sample pre-treatment is available, i.e. preliminary checking of various beverages at shop floors or in the case of suspicion of liquid contamination with toxic metals requiring immediate medical attention. Before putting this method into practice, further research of *LOD*s of other elements as well as the influence of laser wavelength, target material, etc. has to be examined in order to achieve the best possible analytical performance.

Acknowledgments

This work was supported by the ERASMUS+ programme, the Partenariat Hubert Curien/Štefánik programme (No. 35815RH) and the Slovak Research and Development Agency through bilateral program (No. SK-FR-2015-0019).

References

[1] AJTONY, Z. et al. 2008. *Direct sample introduction of wines in graphite furnace atomic absorption spectrometry for the simultaneous determination of arsenic, cadmium, copper and lead content*. Talanta, 76, pp. 627–634.

[2] BAE, D. et al. 2015. *Spreading a water droplet on the laser-patterned silicon wafer substrate for surface-enhanced laser-induced breakdown spectroscopy*. Spectrochimica Acta Part B, 113, pp. 70–78.

[3] BOCKOVÁ, J. et al. 2016. *Determination of metal elements in wines using surface-assisted laser-induced breakdown spectroscopy*. Spectrochimica Acta Part B – submitted for publication.

[4] BUZUKOV, A. A. – POPOV, Y. A. – TESLENKO, V. S. 1969. *Experimental study of explosion caused by focusing monopulse laser radiation in water.*. Zhurnal Prikladnoi Mekhaniki i Tekhnicheskoi Fiziki, 10, pp. 17–22.

[5] CÁCERES, J. O. – LÓPEZ, J. T. – TELLE, H. H. – UREÑA, A. G. 2001. *Quantitative analysis of trace metal ions in ice using laser-induced breakdown spectroscopy*. Spectrochimica Acta Part B, 56, pp. 831–838.

[6] CHENG, H. – LIU, J. – XU, Z., YIN, X. et al. 2012. *A micro-fluidic sub-microliter sample introduction system for direct analysis of Chinese rice wine by inductively coupled plasma mass spectrometry using external aqueous calibration*. Spectrochimica Acta Part B, 73, pp. 55–61.

[7] CREMERS, D. A. – RADZIEMSKI, L. J. 2006. *Handbook of Laser-Induced Breakdown Spectroscopy*. Chichester: John Wiley and Sons Ltd, ISBN 13 978-0-47009299-6 (HB), 283 pp.

[8] CVETKOVIĆ, J. – ARPADJAN, S. – KARADJOVA, I. – STAFILOV, T. 2002. *Determination of thallium in wine by electrothermal atomic absorption spectrometry after extraction preconcentration*. Spectrochimica Acta Part B, 57, pp. 1101–1106.

[9] DE GIACOMO, A. – DELL'AGLIO, M. – DE PASCALE, O. 2004. *Single pulse-laser induced breakdown spectroscopy in aqueous solution*. Applied Physics A, 79, pp. 1035–1038.

[10] DE GIACOMO, A. – DELL'AGLIO, M. – DE PASCALE, O. – CAPITELLI, M. 2007. *From single pulse to double pulse ns-laser induced breakdown spectroscopy under water: Elemental analysis of aqueous solutions and submerged solid samples*. Spectrochimica Acta Part B, 62, pp. 721–738.

[11] DE GIACOMO, A. et al. 2005. *Double-pulse LIBS in bulk water and on submerged bronze samples*. Applied Surface Science, 247, pp. 157–162.

[12] DE GIACOMO, A. et al. 2012. *Effects of the background environment on formation, evolution and*

emission spectra of laser-induced plasmas. Spectrochimica Acta Part B, 78, pp. 1–19.

[13] DESSUY, M. B. et al. 2008. *Method development for the determination of lead in wine using electrothermal atomic absorption spectrometry comparing platform and filter furnace atomizers and different chemical modifiers*. Talanta, 74, pp. 1321–1329.

[14] DOS SANTOS, W. N. L. et al. 2009. *A photo-oxidation procedure using UV radiation/H_2O_2 for decomposition of wine samples — Determination of iron and manganese content by flame atomic absorption spectrometry*. Spectrochimica Acta Part B, 64, pp. 601–604.

[15] FERREIRA, S. L. C. et al. 2007. *Development of method for the speciation of inorganic iron in wine samples*. Analytica Chimica Acta, 602, pp. 89–93.

[16] FERREIRA, S. L. C. et al. 2008. *Direct determination of iron and manganese in wine using the reference element technique and fast sequential multielement flame atomic absorption spectrometry*. Talanta, 74, pp. 699–702.

[17] FRESCHI, G. P. G. et al. 2001. *Simultaneous determination of cadmium and lead in wine by electrothermal atomic absorption spectrometry*. Spectrochimica Acta Part B, 56, pp. 1987–1993.

[18] FRÍAS, S. et al. 2003. *Classification of commercial wines from the Canary Islands (Spain) by chemometric techniques using metallic contents*. Talanta, 59, pp. 335–344.

[19] GALANI-NIKOLAKAKI, S. – KALLITHRAKAS-KONTOS, N. – KATSANOS, A. A. 2002. *Trace element analysis of Cretan wines and wine products*. Science of The Total Environment, 285, pp. 155–163.

[20] GALBÁCS, G. 2015. *A critical review of recent progress in analytical laser-induced breakdown spectroscopy*. Analytical and Bioanalytical Chemistry, 407, pp. 7537–7562.

[21] GALGANO, F. et al. 2008. *Analysis of trace elements in southern Italian wines and their classification according to provenance*. LWT - Food Science and Technology, 41, pp. 1808–1815.

[22] GONZÁLVES, A. et al. 2009. *Elemental fingerprint of wines from the protected designation of origin Valencia*. Food Chemistry, 112, pp. 26–34.

[23] GRUBER, X. – KREGSAMER, P. – WOBRAUSCHEK, P. – STRELI, C. 2006. *Total-reflection X-ray fluorescence analysis of Austrian wine*. Spectrochimica Acta Part B, 61, pp. 1214–1218.

[24] JANTZI, S. C. et al. 2016. *Sample treatment and preparation for laser-induced breakdown spectroscopy*. Spectrochimica Acta Part B, 115, pp. 52–63.

[25] JANZEN, C. et al. 2005. *Analysis of small droplets with a new detector for liquid chromatography based on laser-induced breakdown spectroscopy*. Spectrochimica Acta Part B, 60, pp. 993–1001.

[26] JÄRVINEN, S. T. – SAARELA, J. – TOIVONEN, J. 2013. *Detection of zinc and lead in water using evaporative preconcentration and single-particle laser-induced breakdown spectroscopy*. Spectrochimica Acta Part B, 86, pp. 55–59.

[27] JOS, A. et al. 2004. *Differentiation of sparkling wines (cava and champagne) according to their mineral content*. Talanta, 63, pp. 377–382.

[28] KMENT, P. et al. 2005. *Differentiation of Czech wines using multielement composition – A comparison with vineyard soil*. Food Chemistry, 91, pp. 157–165.

[29] LARA, R. et al. 2005. *Trace element determination of Argentine wines using ETAAS and USN-ICP-OES*. Food and Chemical Toxicology, 43, pp. 293–297.

[30] LAZIC, V. – JOVIĆEVIĆ, S. 2014. *Laser induced breakdown spectroscopy inside liquids: Processes and analytical aspects*. Spectrochimica Acta Part B, 101, pp. 288–311.

[31] METZINGER, A. – KOVÁCS-SZÉLES, É. – ALMÁSI, I. – GALBÁCS, G. 2014. *An assessment of the potential of laser-induced breakdown spectroscopy (LIBS) for the analysis of cesium in liquid samples of biological origin*. Applied Spectroscopy, 68, pp. 789–793.

[32] MIZIOLEK, A. W. – PALLESCHI, V. – SCHECHTER, I. 2006. *Laser-Induced Breakdown Spectroscopy (LIBS): Fundamentals and Applications*. New York: Cambridge University Press, ISBN-13 978-0-521-85274-6, 620 pp.

[33] MORENO, I. M. et al. 2007. *Differentiation of two Canary DO red wines according to their metal content from inductively coupled plasma optical emission spectrometry and graphite furnace atomic absorption spectrometry by using Probabilistic Neural Networks*. Talanta, 72, pp. 263–268.

[34] MORENO, I. M. et al. 2008. *Determination of Al, Ba, Ca, Cu, Fe, K, Mg, Mn, Na, Sr and Zn in red wine samples by inductively coupled plasma optical emission spectroscopy: Evaluation of preliminary sample treatments*. Microchemical Journal, 88, pp. 56–61.

[35] POHL, P. 2007. *What do metals tell us about wine?* Trends in Analytical Chemistry, 26, pp. 941–949.

[36] POHL, P. 2009. *Suitability of solid phase extraction and flame atomic absorption spectrometry for manganese partitioning in red wines*. Food Chemistry, 114, pp. 996–1001.

[37] POHL, P. – PRUSISZ, B. 2009. *Application of tandem column solid phase extraction and flame atomic*

absorption spectrometry for the determination of inorganic and organically bound forms of iron in wine. Talanta, 77, pp. 1732–1738.

[38] RADZIEMSKI, L. J. – CREMERS, D. A. 1989. *Laser-Induced Plasma and Applications*. New York: Marcel Dekker, ISBN 0-8247-8078-7 (HB), 464 pp.

[39] SCHIAVO, D. – NEIRA, J. Y. – NÓBREGA, J. A. 2008. *Direct determination of Cd, Cu and Pb in wines and grape juices by thermospray flame furnace atomic absorption spectrometry*. Talanta, 76, pp. 1113–1118.

[40] SEEGER, T. S. et al. 2015. *Feasibility of dispersive liquid–liquid microextraction for extraction and preconcentration of Cu and Fe in red and white wine and determination by flame atomic absorption spectrometry*. Spectrochimica Acta Part B, 105, pp. 136–140.

[41] SERAPINAS, P. et al. 2008. *Step by step approach to multi-element data analysis in testing the provenance of wines*. Food Chemistry, 107, pp. 1652–1660.

[42] SOBRAL, H. – SANGINÉS, R. – TRUJILLO-VÁZQUES, A. 2012. *Detection of trace elements in ice and water by laser-induced breakdown spectroscopy*. Spectrochimica Acta Part B, 78, pp. 62–66.

[43] ŠELIH, V. S. – ŠALA, M. – DRGAN, V. 2014. *Multi-element analysis of wines by ICP-MS and ICP-OES and their classification according to geographical origin in Slovenia*. Food Chemistry, 153, pp. 414–423.

[44] XIU, J. et al. 2013. *Indirect laser-induced breakdown of transparent thin gel layer for sensitive trace element detection*. Applied Physics Letters, 102, pp. 1–5.

[45] XIU, J. et al. 2014. *Feasibility of wear metal analysis in oils with parts per million and sub-parts per million sensitivities using laser-induced breakdown spectroscopy of thin oil layer on metallic target*. Spectrochimica Acta Part B, 91, pp. 24–30.

[46] YAROSHCHYK, P. – MORRISON, R. J. S. – BODY, D. – CHADWICK, B. L. 2005. *Quantitative determination of wear metals in engine oils using laser-induced breakdown spectroscopy: A comparison between liquid jets and static liquids*. Spectrochimica Acta Part B, 60, pp. 986–992.

[47] YAROSHCHYK, P. – MORRISON, R. J. S. – BODY, D. – CHADWICK, B. L. 2005. *Quantitative determination of wear metals in engine oils using LIBS: The use of paper substrates and a comparison between single- and double-pulse LIBS*. Spectrochimica Acta Part B, 60, pp. 1482–1485.

[48] ZOROV, N. B. – GORBATENKO, A. A. – LABUTIN, T. A. – POPOV, A. M. 2010. *A review of normalization techniques in analytical atomic spectrometry with laser sampling: From single to multivariate correction*. Spectrochimica Acta Part B, 65, pp. 642–657.